AN EXPERIMENTAL INVESTIGATION OF THE THERMAL BEHAVIOR OF A FIXED BED REGENERATOR

A Thesis

by

JAY ROHIT VERLEKAR

Submitted to the Graduate and Professional School of
Texas A&M University
in partial fulfillment of the requirements for the degree of

MASTER OF SCIENCE

Chair of Committee,	Michael B. Pate
Committee Members,	David E. Claridge
	Maria D. King
Head of Department,	Guillermo Aguilar

May 2023

Major Subject: Mechanical Engineering

ABSTRACT

Heating, Ventilation and Air-Conditioning (HVAC) systems consume large amounts of energy to maintain acceptable thermal environments for occupants; therefore, it becomes important to develop energy efficient systems to support this primary HVAC system goal. The Fixed Bed Regenerator (FBR) is a type of energy recovery system that offers preconditioning of fresh supply air without compromising on Indoor Air Quality (IAQ). This device consists of a cylindrical core made of ceramic for thermal energy storage and laced with numerous hollow channels for air flow so the device can act as a regenerative heat exchanger. The FBR also contains a reversible fan that facilitates air movement between the outdoors and indoors by alternating channel airflow in two directions. The ceramic core absorbs energy from the hot outside air flowing through channels during the supply cycle, which spans 50 seconds for this particular unit, thus cooling fresh outdoor air before it discharges to the indoor space. Next, the core transfers energy to the indoor space air flowing back through the channels during the exhaust cycle, which also spans 50 seconds. Thus, a complete cycle, which consists of a combination of the supply cycle and the exhaust cycle, lasts 100 seconds. The objective of this project is to evaluate the thermal behavior, the core charging and discharging phenomenon, and the effectiveness of the FBR for a range of indoor-to-outdoor temperature differences.

Before taking data for analysis, it was necessary to develop a methodology that ensures the onset of pseudo steady state after an initial FBR startup by monitoring how long it takes the core temperatures to stabilize; it was determined that pseudo steady state was reached after about 16 minutes for all cases. As a first step in the FBR analysis, the temperature change of air flowing through the core provided an indication of the FBR effectiveness. For example, at an outdoor-to-indoor temperature difference of ΔT_{max} =25°F, the inlet-to-outlet air temperature difference during the supply cycle decreased from 22.9°F to 11.8°F from the cycle beginning to the end. For the exhaust cycle, this inlet-to-outlet temperature difference decreased from 15.4°F at the cycle beginning to 8.6°F at the end. These decreasing temperature differences from the start to the end of both cycles is an indicator that the core has a decreasing ability to exchange thermal energy with the air or, in terms of this FBR study, a decreasing effectiveness as time passes during a cycle. For example, in the ΔT_{max}=25°F case, the effectiveness, which is calculated from temperature data,

decreased from 0.90 at the start to 0.47 at the end of the supply cycle, and similarly from 0.80 to 0.39 for the exhaust cycle. The effect that ΔTmax has on mean and peak effectiveness was also evaluated. An analysis of the complete cycle, which is a combined supply and exhaust cycle, showed that the mean effectiveness increased slightly from 0.50 at ΔTmax=20°F to 0.53 at ΔTmax=30°F. The peak effectiveness showed a similar trend of a slight increase from 0.85 at ΔTmax=20°F to 0.94 at ΔTmax=30°F. Thus, it was determined that, among the three ΔTmax samples analyzed, the optimal operating conditions for the Fixed Bed Regenerator were at ΔTmax=30°F.

ACKNOWLEDGEMENTS

I would like to thank my committee chair, Dr. Pate, and my committee members, Dr. Claridge and Dr. King, for their guidance and support throughout the course of this research.

I would also like to acknowledge the technical guidance from all my friends and colleagues at the RELLIS Energy Efficiency Laboratory. In particular, the contributions of Dr. James F. Sweeney, Jimmie Smith and Tristan Smith were extremely important in ensuring the continuous progress and completion of my thesis.

I am truly grateful for all the support and encouragement from my girlfriend Ketki Kulkarni, who spent significant time and efforts in ensuring that I manage my graduate studies efficiently and that I am in a good headspace.

Finally, a big thank you to my family in India – my parents (Anupama Verlekar & Rohit Verlekar), sister (Sara Verlekar) and my grandmother (Anita Verlekar). Their positivity and unconditional love played a big role in keeping me constantly motivated throughout my graduate studies.

CONTRIBUTORS AND FUNDING SOURCES

Contributors

This work was supervised by a thesis committee consisting of Dr. Michael Pate and Dr. David E. Claridge of the Department of Mechanical Engineering and Dr. Maria D. King of the Department of Biological and Agricultural Engineering.

Funding Sources

Graduate study was supported by a Graduate Research Assistantship from RELLIS Energy Efficiency Laboratory.

TABLE OF CONTENTS

Page

LIST OF FIGURES

Page

LIST OF TABLES

Page

CHAPTER 1: INTRODUCTION

Heating, Ventilation and Air Conditioning (HVAC) systems play an important role in maintaining occupant comfort in buildings/ indoor spaces. Humans have certain requirements of thermal conditions around them; for instance, they need a specific range of air temperatures, humidity levels, air movement and air purity in their surroundings so that their bodies can function effectively both physically and mentally. It is to satisfy these thermal requirements that HVAC systems operate, and they consume a significant proportion of energy in doing so. In order to maintain an optimum level of air purity, which is characterized in terms of Indoor Air Quality (IAQ), there needs to be a regular supply of conditioned fresh air sourced from the outdoors while simultaneously ensuring that the stale air from the indoors is exhausted. However, the process of conditioning fresh outdoor supply air on a continuous basis that comprises cooling and dehumidification (in summers) and heating and humidification (in winters) is an extremely energy intensive process. Keeping in mind the current trends of energy consumption in buildings for space heating and cooling, which are anticipated to increase by huge margins in the next few decades, it becomes imperative to develop systems that reduce energy requirements by making more energy efficient.

1.1 Air-to-Air Energy Exchangers and their Categories

In response to the above scenario, the development of Air-to-Air Energy Exchangers (AAEEs) systems can meet the objective of energy efficiency while ensuring that the Indoor Air Quality is not affected. These systems facilitate energy exchange between the exhaust air stream that flows from the indoors to the outdoors and the supply air stream that flows from the outdoors to the indoors, thus preconditioning the supply air before it enters the primary system responsible for space heating, cooling and ventilation, which can be in the form of an air conditioner, a furnace, or a heat pump. This preconditioned air that enters a primary HVAC system reduces the energy consumption of the system since a part of the load is met by the energy recovery process facilitated by the AAEEs.

AAEEs are broadly divided into two categories, namely recuperative types and regenerative types. The recuperative type system is characterized by direct energy exchange occurring between the supply and exhaust air streams (simultaneously flowing in parallel channels) through a conducting medium placed between them. The regenerative type exchanger is characterized by the two air streams having the same channel to flow through, although in periodic intervals. This exchanger type is further subdivided into two categories of rotary and stationary. A rotary type heat exchanger consists of a rotating wheel that is the medium for heat exchange between the two air streams, while the stationary, or fixed type, consists of a fixed core along with a reversible fan that facilitates the periodic flow of the supply and exhaust airstreams in opposite directions.

1.2 Literature Review

Fixed bed regenerators (FBRs) are an important component of heating, ventilation, and air conditioning (HVAC) systems. The high thermal storage capacity of FBRs makes them an excellent choice for HVAC systems; they can store a significant quantity of thermal energy in a relatively small volume. When there is minimal demand, thermal energy can be stored in TES systems using FBRs, which can then be released when there is high demand (Chen et al., 2018). This can lessen the need for on-demand heating or cooling, which can help to lower the energy consumption of HVAC systems.

Using FBRs in HVAC systems has another benefit due to their capacity to deliver a steady and constant thermal output, which in this case refers to the quality of preconditioned air. FBRs are a great option for heating and cooling applications since they can produce a steady thermal output over an extended length of time (Zhu et al., 2020). As a result, the indoor climate can be kept comfortable while using less energy.

The effectiveness of fixed bed regenerators (FBRs) in HVAC systems depends on a number of factors, including the type of working fluid, the operating conditions, and the design of the FBR itself. In general, the effectiveness of FBRs can be improved by increasing the heat transfer area, increasing the thermal conductivity of the FBR material, and optimizing the operating conditions (Li et al., 2016).

The effectiveness of FBRs in HVAC systems has been the subject of past research studies, including one by Zhang et al. (2016) who found that effectiveness improved with increasing mass

flow rate and decreasing inlet temperature. Similar to this, Chen et al. (2018) investigated the performance of an FBR and found that the operating temperature, the heat transfer area, and the thermal conductivity of the FBR material all had an impact on the FBR's effectiveness.

Wu et al. (2019) suggested a new design for an FBR that included phase change materials (PCMs) to increase the FBR's ability to store energy and effectiveness. They discovered that the addition of PCMs increased the FBR's thermal storage capacity by up to 80% and enhanced the system's overall effectiveness.

Graphene and carbon nanotubes are examples of innovative materials with excellent thermal conductivity that can be used to improve the effectiveness of FBRs. For instance, Gao et al. (2020) evaluated the use of graphene oxide (GO) in an FBR for thermal energy storage and discovered that the addition of GO considerably increased the FBR's thermal conductivity and the system's overall effectiveness.

One study by Karami et al. (2019) investigated the use of a fixed bed regenerator for preheating the incoming fresh air in a commercial building. According to the research, the regenerator could recover up to 60% of the waste heat from the exhaust air stream and pre-heat the incoming fresh air to a temperature of 25°C, which led to a 29% reduction in energy consumption. Also, the heat exchanger's (core) temperature changed over time, reaching its highest point at the start of operation when the exhaust air stream temperature was also at its peak. As the temperature of the discharge air stream dropped over time, the heat exchanger's temperature also followed the same trend.

Another study by Zhao et al. (2016) investigated the use of a fixed bed regenerator for preheating the incoming fresh air in a residential building. According to the research, the regenerator was able to recover up to 70% of the waste heat from the exhaust air stream and pre-heat incoming fresh air to a temperature of 25°C, which resulted in a 32% reduction in energy consumption.

The temperature vs. time variations of the core in a fixed bed regenerator are influenced by its design, the thermal properties of the materials used in it, the flow rates of the exhaust and fresh air streams, and the operating conditions that prevail. In general, the temperature vs time variations of the heat exchanger in a fixed bed regenerator depend on several factors and should be carefully evaluated for each application. Understanding these variations can aid in optimizing the system's design, functionality, and general performance.

FBRs have some drawbacks despite the numerous benefits that they offer. Their relatively low thermal conductivity, which results in a reduced heat transfer rate between the FBR and the working fluid and, in turn, reduced the effectiveness of the system (Chen et al., 2018).

1.3 Scope and Objectives

The purpose of this project is to understand the thermal behaviour, evaluate the performance and determine the optimal conditions of operation of a Fixed Bed Regenerator by designing and building a temperature controlled test facility, and then generating data from the experiments conducted. The temperature trends of the air and of the ceramic core, as well as the sensible effectiveness trends are analysed to understand how the core interacts with the flowing air in terms of energy transfer and to understand how the core charges and discharges during supply and exhaust cycles respectively. The sensible effectiveness is an important performance parameter used as a measure of the thermodynamic and heat transfer performance of the FBR, being indicative of the energy transfer occurring between the air and the core with respect to the maximum energy transfer possible. It is calculated as follows:

$$\varepsilon = \Delta T \; / \; \Delta T \; max$$

Here ΔT is the absolute temperature difference between the moving air at the inlet and outlet and $\Delta T \; max$ is the maximum temperature difference that is possible to attain.

Another aspect of this study is determining the onset of pseudo-steady state during the operation. The pseudo-steady state occurs when the air and the core temperature variations with respect to time during successive supply and successive exhaust cycles show a cyclical nature. This state is different from a pure steady state in which there is no variation of the temperature with respect to time, and a pure unsteady state in which there is a continuous temperature variation with respect to time, but no observed cyclical nature.

Several plots are generated from the collected data to understand these temperature and sensible effectiveness trends, such as air temperature vs cycle time, core temperature vs cycle time, core

temperature vs longitudinal core position, core temperature vs radial core position, comparison of air and core temperatures vs cycle time, sensible effectiveness vs cycle time, etc. An integral part of this thesis is understanding how all these trends that encompass several thermodynamic parameters vary when the indoor (lab space) and outdoor (chamber space) temperatures are varied. This comparative study eventually leads to determination of the optimal operating conditions for the FBR, which is when peak performance is observed.

1.4 Overview of Thesis Organization

Chapter 2 outlines the description of the experimental setup along with the relevant procedures for conducting tests on the facility. The different parts of the setup consist of the Data Acquisition System (DAQ), temperature and pressure measurement, heating element at the entrance of intake duct, intake fan and pressure relief, LabView graphical interface and the PID controller. The DAQ system ensures that data measured by temperature and pressure sensors is eventually written to an Excel file for further analysis. The heating element raises the temperature of the air entering the chamber to a specific value which is set on the PID controller. The intake fan drives the heated air into the chamber and the manual adjustments on the pressure relief ensure that the pressure inside the chamber measures zero inches of water. The graphical interface on LabView helps monitor the temperature variations with time and helps in ensuring that the desired temperature has been attained.

Chapter 3 focusses on the theoretical aspects of the Fixed Bed Regenerator through the application of the fundamentals of thermodynamics and heat transfer in order to explain the energy transfer process occurring between the core and the air. The chapter is divided into three sections -the first one focusing on the heat transfer considering the core element as the control volume, the second one explaining the heat transfer considering the air element (in contact with the core element) as the control volume, and the last one explaining the energy exchange occurring between the core and the flowing air, which is essentially the same as the heat transfers discussed in the first two sections. These sections consist of derivation of the governing equations based on First Law of Thermodynamics and convective heat transfer.

Chapter 4 shows the results of the in-depth analysis performed on the experimental data from the test facility (that simulates real-life operating scenarios) to understand the thermal behavior of the FBR. This is understood in terms of air and core temperature trends as well as effectiveness trends. The air discharge temperature-time trends, effectiveness vs cycle time, core longitudinal and radial temperature distributions w.r.t core positions, and comparison of air discharge temperature with core temperature variation vs cycle time are some examples of the plots obtained from the experimental data. The trends observed from these plots are analyzed and reasonings based on thermodynamics and heat transfer concepts are developed to justify these trends or to explain why certain trends do not align with theoretical expectations.

Chapter 5 investigates the influence of the temperature difference between the indoors (lab space) and outdoors (chamber space) on the thermal behavior of the FBR. It looks at different ways of analyzing how ΔT_{max} (the temperature difference between indoors and outdoors) influences FBR behavior – comparison at different ΔT_{max} values is made between the air and core temperature swings on either ends of the FBR unit, mean core temperatures, air discharge temperatures during supply and exhaust, effectiveness variation with time, mean and peak effectiveness trends, core temperature variation with time, core temperature variation with longitudinal distance, etc. The mean and peak effectiveness trends are analyzed to determine the optimal operating conditions at which the FBR is at peak performance, where the performance metric used is effectiveness. As done in the previous experimental analysis, there are reasonings developed to justify the trends observed or to explain why certain trends do not align with theoretical expectations.

CHAPTER 2: EXPERIMENTAL SETUP AND METHODOLOGY

The focus of this thesis project is an experimental evaluation of a Fixed Bed Regenerator, or FBR, which is a specialized type of fixed, regenerative AAEE system. Therefore, it was necessary to build an experimental setup that could in turn be used for testing and evaluating FBRs at real-world conditions.

2.1 Fixed Bed Regenerator: Working Principle and Experimental Setup

This FBR device that was integrated into the experimental test facility consists of a cylindrical ceramic core with numerous hollow channels for air flow that together form a regenerative heat exchanger. The channels of the ceramic core can be seen in the chamber side view (i.e, end view) in Figure 2.1. The side/top view of the core also in Figure 2.1 shows that the core with channels is approximately 3 inches long, which is convenient for installing in a wall with air entering and exiting the core perpendicular to the wall. Furthermore, a reversible fan is mounted at the end of the core on the lab side. This fan facilitates air movement between the outdoors and indoors by alternating or cycling the airflow in two directions through the core channels (shown in Figure 2.1). Specifically, when the fan operates so that air movement is from the simulated outdoors to the indoors, it is referred to as the supply cycle. After a pre-set time interval, the fan reverses its direction of rotation and the air flows from the indoors to the outdoors, which constitutes the exhaust cycle. As air flows through the hollow channels of the core in either cycle, thermal energy is exchanged between the air and the ceramic core. For example, during the supply cycle, as the fresh air moves from the hot outdoors to the indoors, thermal energy transfer heats the core, thus cooling the air prior to being discharged to the indoor space. During this supply cycle, the core is said to undergo “charging” as it heats up. During the exhaust cycle, the stale air moving from the indoors to the outdoors absorbs thermal energy from the core, thus increasing the temperature of the flowing air. At the same time, the core temperature drops as it loses thermal energy to the air and in this situation, the core is said to undergo “discharging”. The above process of a supply cycle followed by an exhaust cycle represents one complete cycle. An operating FBR repeats this complete cycle according to pre-set time intervals, which in the case of this study was about 100 seconds.

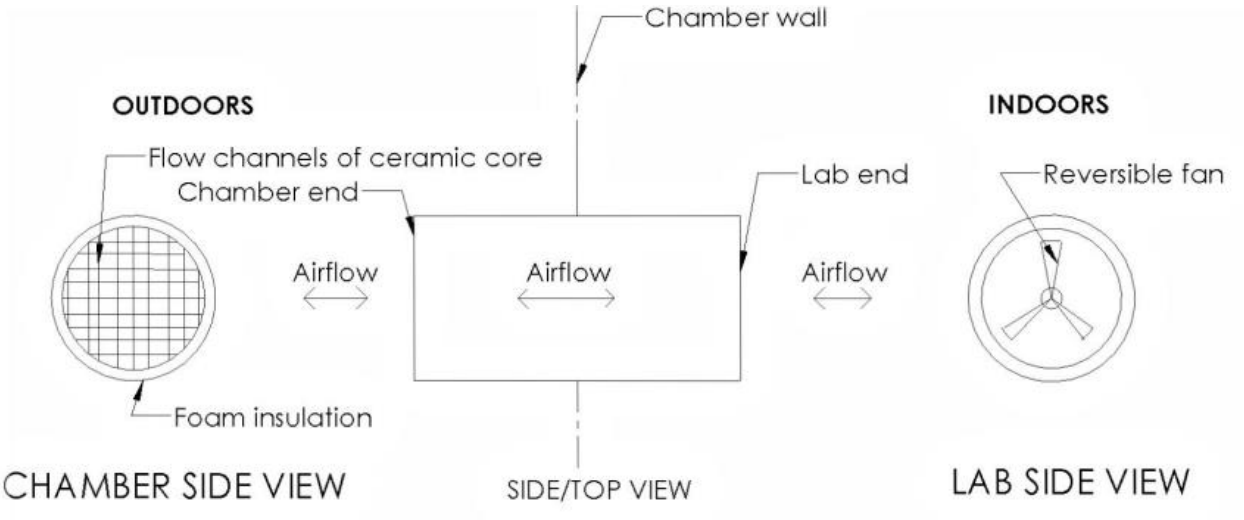

Figure 2.1: 2-D sketch of the FBR unit as seen from the chamber side, laboratory side and from the side/top.

The experimental set up is intended to test and evaluate an operating FBR using actual operating conditions. In order to set and control simulated outdoor conditions, a cube-shaped chamber assembly (shown in Figure 2.2) was constructed with an intake duct for heated air to enter the chamber and an exhaust duct for the relief air to exit. Upstream of the intake duct is an electric coil that heats the air to a predetermined temperature. The chamber simulates hot, outside ambient conditions while the laboratory space simulates the cooler indoor conditions. Downstream of the exhaust duct (shown in Figure 2.4) is the pressure relief fan whose speed is manually controlled so as to maintain a zero pressure differential between the chamber and laboratory space. On one of the walls of the chamber is a cut out that houses the Fixed Bed Regenerator (shown in Figure 2.5) being tested, while exchanging air between the hot-air chamber space representing the outdoor and the laboratory space representing a typical indoor space.

Using the laboratory as a typical indoor space is convenient because it is a large occupied space (shown in Figure 2.3 is a view of FBR unit from the lab or supply side) whose temperature is fixed and not easily varied. The reason for the chamber simulating the hot, outside ambient conditions is that it has sensors and heating units that allow for controlled, elevated temperature representation of a range of outdoor temperatures.

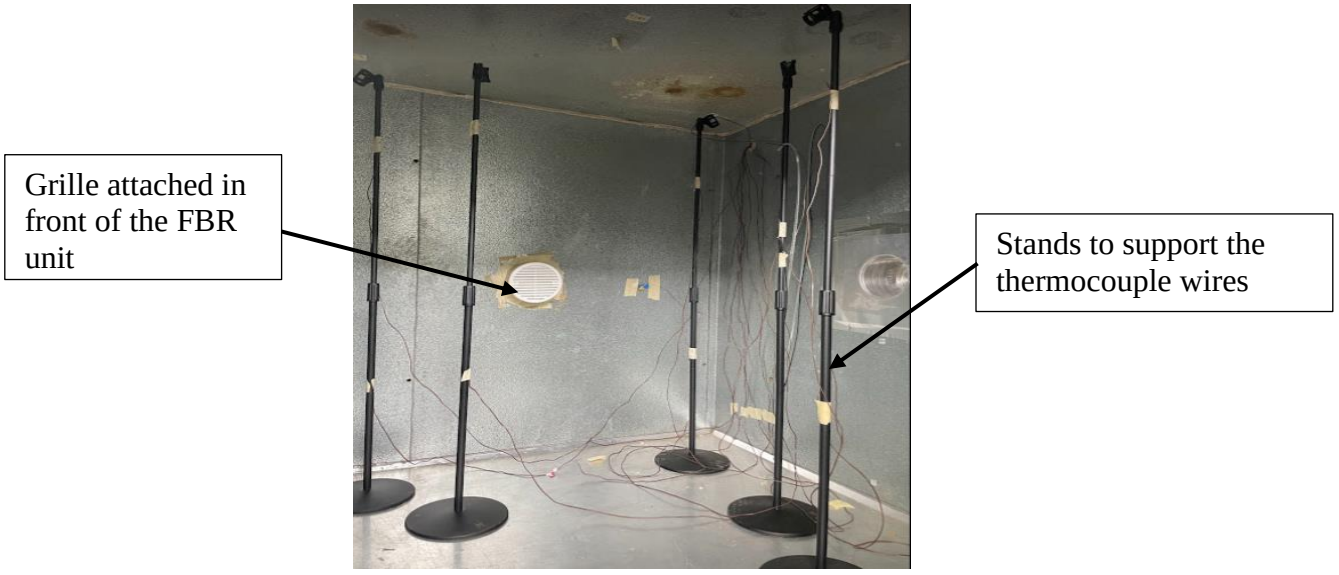

Figure 2.2: Inside of the FBR chamber, with thermocouples installed on the stands to measure chamber temperature and the FBR unit behind the white-colored grille.

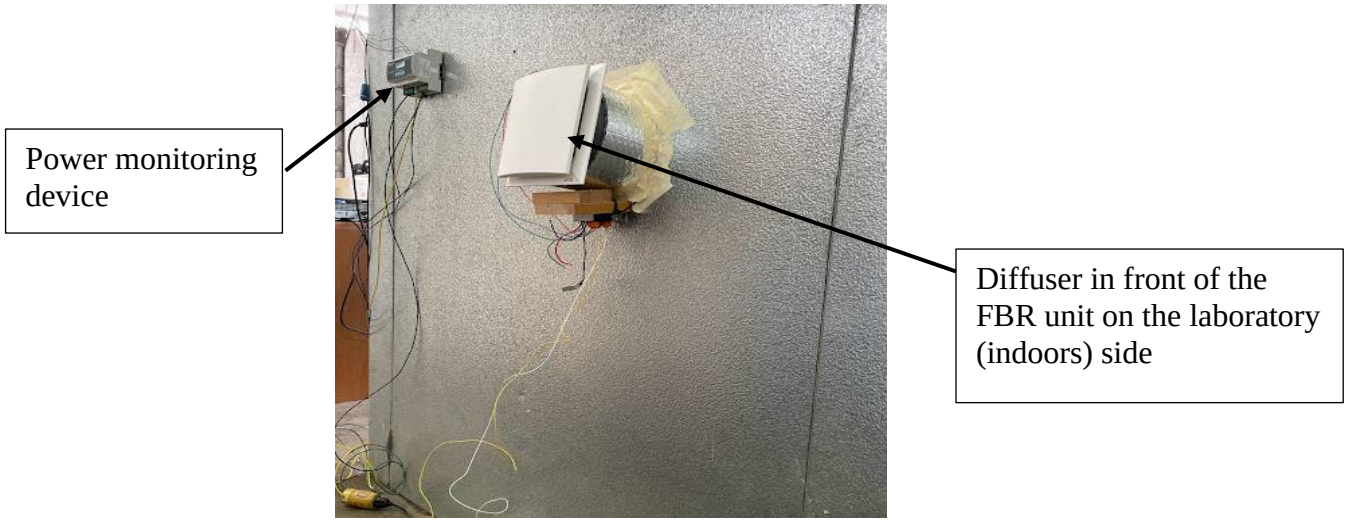

Figure 2.3: The FBR unit from the supply (lab) side

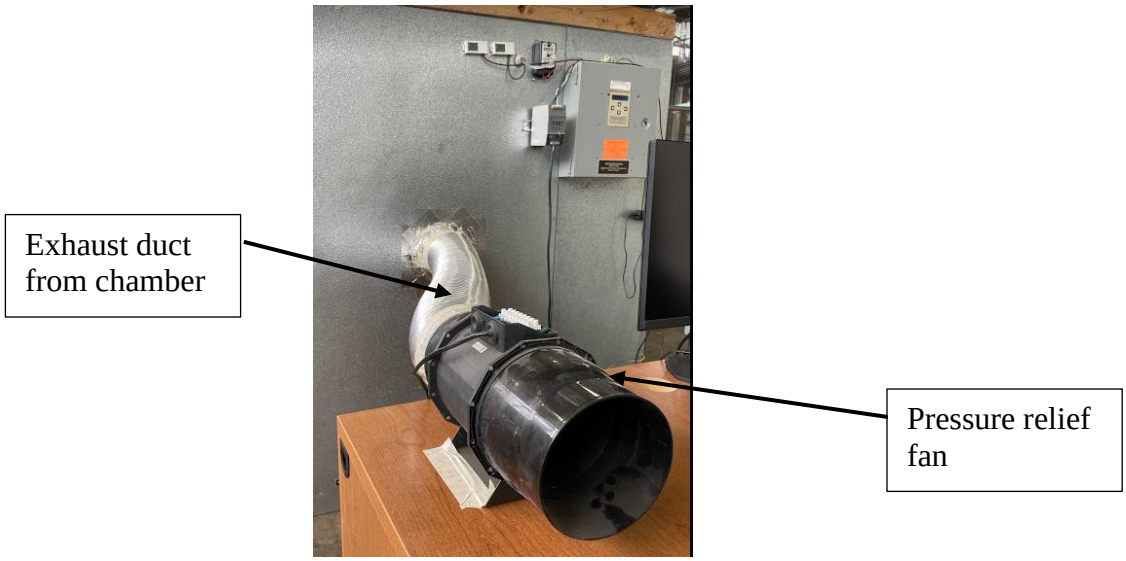

Figure 2.4: Exhaust duct along with pressure relief fan to regulate chamber pressure

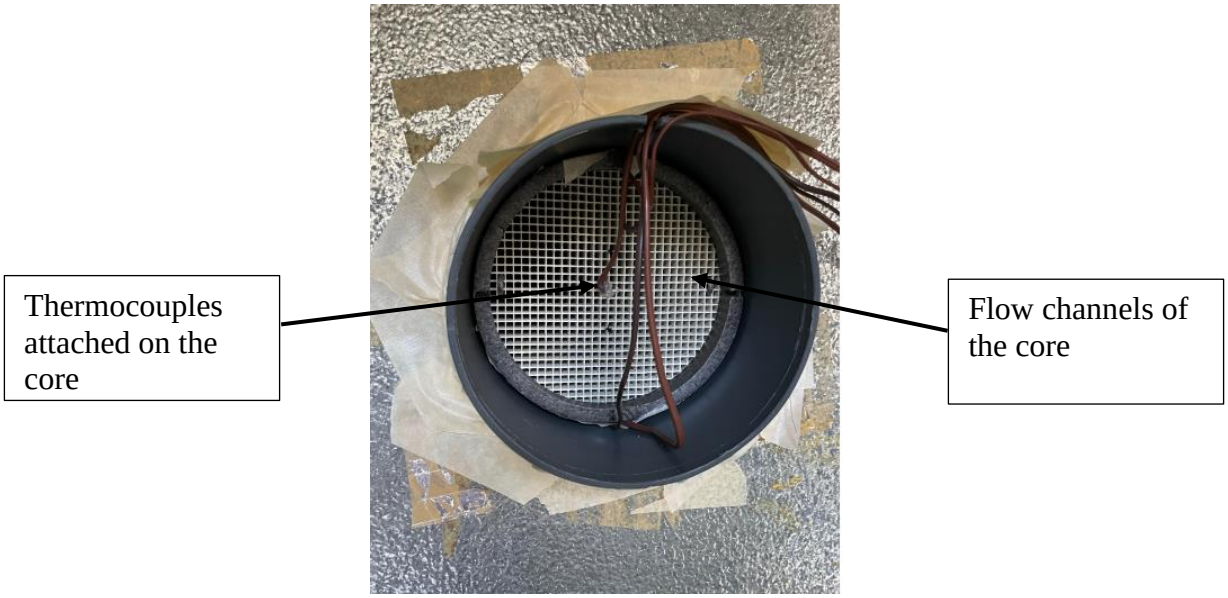

Figure 2.5: FBR core on the chamber side, along with thermocouples attached at the centre, top and the bottom.

2.2 Data Acquisition System (DAQ)

In order to get the experimental setup ready for testing, the thermocouples that measure the air and core temperatures and the pressure sensor that is used to determine the pressure conditions inside of the chamber are fed into the data acquisition system. The data acquisition system for the FBR

facility is a physical implementation of the code formulated in LabView which ensures that the data measured by the temperature and pressure sensors is eventually written to an Excel file for further analysis. The pressure sensor is wired into a NI 9205 analog input module which converts the voltage return of the sensor into recordable data through a pressure to voltage conversion ratio. The various thermocouples are connected to the NI 9213 and NI 9211 thermocouple modules (shown in Figure 2.6). These modules record the temperature from the T-type thermocouples by measuring the resistance of the soldered tip between the aluminium and copper wires of the thermocouple.

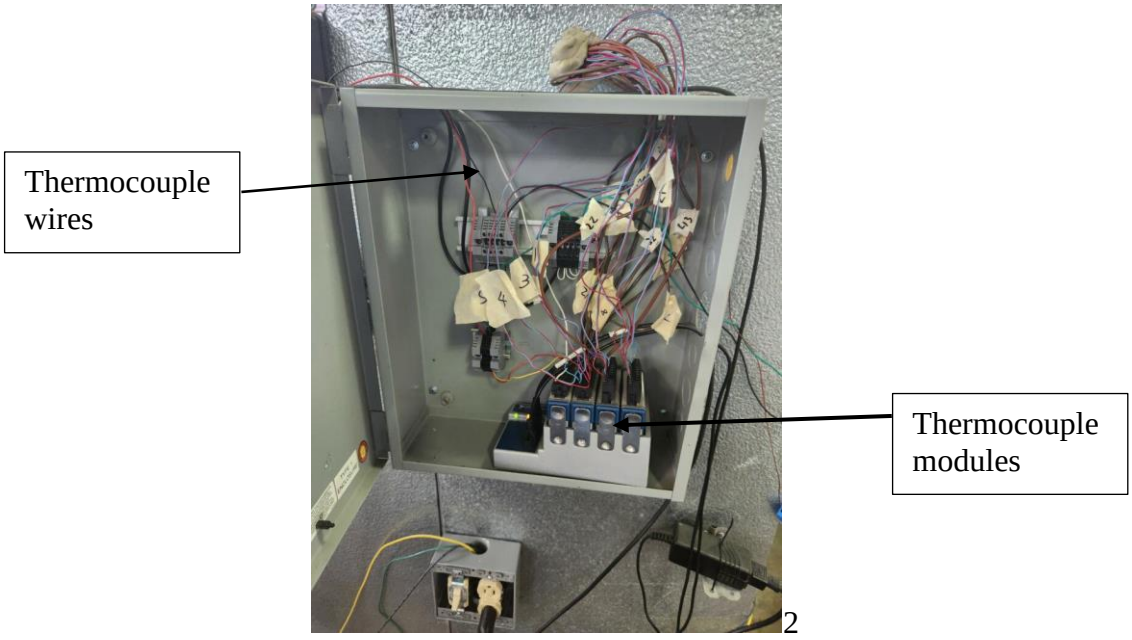

Figure 2.6: Data Acquisition System panel, consisting of the various T-type thermocouples connected to the thermocouple modules

2.3 Temperature Measurement

Six thermocouples are used to measure the temperature throughout the chamber and are averaged to determine the simulated outdoor temperature. Two more thermocouples are suspended mid-air on either side of the FBR unit to measure the air temperature on both the indoor and outdoor sides of the test setup. Sixteen more thermocouples are placed according to a specific arrangement on

the ceramic core of the FBR unit (shown in Figure 2.7) in order to measure the distribution of core temperature longitudinally, radially and with time.

Figure 2.7: FBR core from the chamber side with thermocouples attached at 16 points

2.4 Heating Element

The chamber room is filled with hot air of the intake duct that it flows through which has the heating element at its entrance (shown in Figure 2.8). The heating element is basically a large 480 V electric coil whose purpose is to increase the air temperature in the chamber space so that the desired temperature difference between the simulated outdoor and indoor conditions is attained.

Figure 2.8: Heating element inside of the rectangular intake duct

2.5 Intake Fan and Pressure Relief

Downstream of the heating element is the intake fan (shown in Figure 2.9) that drives the flow of the heated air to the interior of the chamber. Accompanied by this is the pressure relief fan placed downstream of the exhaust outlet (shown in Figure 2.10) that has its speed manually adjusted from time to time in order to ensure that the pressure differential between the chamber and laboratory space is zero, which is important for keeping the flow through the FBR constant.

Figure 2.9: Intake Fan attached downstream of the heating element

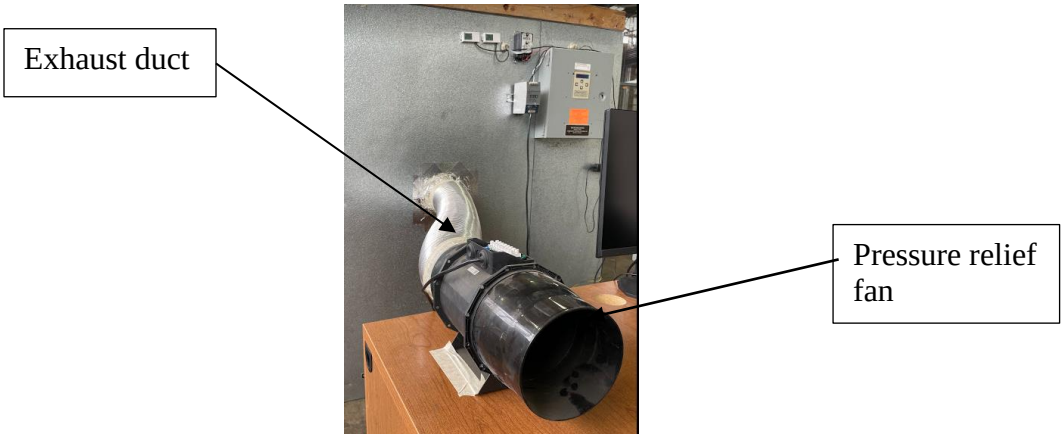

Figure 2.10: Exhaust duct along with pressure relief fan to regulate chamber pressure

2.6 LabView Graphical Interface and PID controller

In order to run a test, the temperature of the heater would need to be set with the help of a PID controller. Typically, this setting should exceed the desired temperature by approximately 10 °F keeping in mind the size of the chamber and the heat losses taking place during the process of hot air accumulation. The graphical interface on LabView helps to ensure that the desired temperature is reached. This interface acts as a platform to continuously monitor the temperature trends on a real-time basis that help in identifying anomalies and in taking corrective action to ensure quality data generation. For instance, the graphical interface showing a sudden drop in chamber space temperature is indicative of an abnormality in test conditions that call for corrective action such as ensuring that there is no air leakage from the chamber space. When the chamber space temperature reaches approximately 2 °F above the desired temperature, the exhaust fan would be turned on and adjusted until the average pressure in the chamber is zero inches of water. This in turn would lower the chamber temperature slightly and help attain the desired value by exhausting some of the heat.

The above mentioned procedures concerned with different instrumentation and equipment ensure that the set up is ready for experimentation, after which the FBR unit is powered and the testing begins.

2.7 Approach to Data Analysis

During the analysis of the experimental data, it is important to break the raw data down into sections based on cyclical periods of supply and exhaust, which organizes data that can then be easily plotted with the desired parameters. Categorizing the raw data into supply and exhaust cycles is done by monitoring the air discharge temperatures on the laboratory end (represents indoors) and the chamber end (representing outdoors) of the FBR unit respectively. A supply cycle is characterized by increasing discharge temperatures on the laboratory side and a sudden dip in temperatures indicates switching of the cycle from supply to exhaust. On the other hand, an exhaust cycle is characterized by decreasing discharge temperatures on the chamber side and fluctuation in these temperatures indicate cycle switching from exhaust back to supply. This categorization of supply and exhaust cycle data is necessary not only for calculating the effectiveness, wherein the temperature difference ΔT calculation is different in the case of supply and exhaust, but also for thorough analysis of the temperature and effectiveness trends for a complete cycle (i.e, one supply cycle followed by one exhaust cycle) during the pseudo-steady state period.

The determination of the onset of pseudo-steady state was, in earlier experiments, done by looking at the degree of alignment of temperature-time variations during successive supply and successive exhaust cycles. However, in the latest experiments, this practice was replaced by one where core temperature – time trends were studied and the onset was determined by visualizing at what point this curve stabilized and had a periodic nature.

CHAPTER 3: THEORY OF FBR AND GOVERNING EQUATIONS

To summarize the concepts which govern the working of the Fixed Bed Regenerator:

1. It is a cyclical heat recovery device with alternate periods of supply and exhaust cycle, with a single channel for both supply and exhaust air streams.
2. Hot, fresh air flows from the outdoors through the channels of the ceramic core, dissipating heat to it as it passes through and gradually cooling down as it enters the outlet on the supply side. This consists of the supply cycle.
3. Stale air flows from the indoors to the outdoors through the channels of the core, absorbing heat from the "charged" core and gradually heating up as it enters the outlet on the exhaust side.
4. Thus, the core is continuously exchanging energy in the form of heat with the air flowing through its channels.

This chapter is intended to explain, through the application of the fundamentals of thermodynamics and heat transfer, the energy transfer process occurring between the core and the air in order to facilitate the working of the Fixed Bed Regenerator. The chapter is divided into three sections - the first one focussing on the heat transfer considering the core element as the control volume, the second one explaining the heat transfer considering the air element as the control volume, and the last one explaining the energy exchange occurring between the core and the flowing air, which is essentially the same as the heat transfers discussed in the first two sections.

3.1 Heat Transfer Considering Core Element as the Control Volume

For the purpose of this analysis, let us consider that the cylindrical core of of length L is broken down into 'n' elements, each having length 'x' and air is flowing past one surface of this element. This core element, with the air control volume in its contact is shown in Figure 3.1. Considering the case of the exhaust cycle for this analysis, the core will be dissipating heat $\dot{q}(conv)$ to the air passing through.

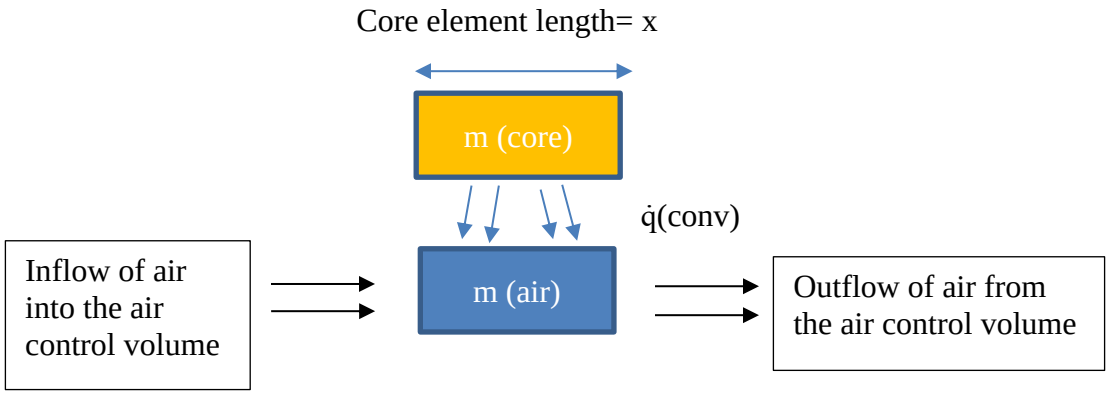

Figure 3.1: Schematic of the control volumes of the core element and the air element in contact with it, with the convective heat transfer taking place between the two.

Given below is the equation governing the First Law of Thermodynamics that is relevant to this arrangement:

$$\frac{dE}{dt} = \dot{q}(in) - \dot{q}(out) + \dot{W}(in) - \dot{W}(out) + \dot{m}(in)(h + v^2/2 + gz)(in) - \dot{m}(out)(h + v^2/2 + gz)(out)$$

Where:

$\dot{q}(in)$: Rate of heat absorption by the control volume.

$\dot{q}(out)$: Rate of heat dissipated from the control volume.

$\dot{W}(in)$: Work done on the control volume.

$\dot{W}(out)$: Work done by the control volume.

$\dot{m}(in)$: Mass flowing into the control volume.

$\dot{m}(out)$: Mass flowing out of the control volume.

$(h + v^2/2 + gz)(in)$: enthalpy, kinetic and potential energies of the inflow per unit mass.

$(h + v^2/2 + gz)(out)$: enthalpy, kinetic and potential energies of the outflow per unit mass.

For this control volume, the heat gained, work transfer, inflow and outflow of fluid all equal zero.

$\dot{q}(in) = \dot{W}(in) = \dot{W}(out) = \dot{m}(in) = \dot{m}(out) = 0$

Simplifying the first law equation, we get

$$\frac{dE}{dt} = \frac{d(mu)}{dt} = m.\frac{du}{dt} = m.c.dTc/dt = \dot{q}(out)$$

Where:

u: Internal energy of the core element per unit mass

Tc: Temperature of the core element

The above equation governs the heat transfer occurring between the air and the core with the core element as control volume.

3.2 Heat Transfer Considering Air Element as the Control Volume

The control volume through which the air passes can be considered to be adjacent to, and in contact with the core element analyzed previously, as shown in Figure 3.1. For this control volume,

$\dot{m}(in) = \dot{m}(out) = \dot{m}(air)$

From the general first law equation, the unsteady term dE/dt can be neglected because the mass of air m(air) contained within the control volume can be assumed to be negligible. Further, in this control volume, there is no work transfer present or any change in kinetic or potential energies of the air inflow and outflow.

$dE/dt = \dot{q}(out) = \dot{W}(in) = \dot{W}(out) = 0$

$(v^2/2 + gz)(in) = (v^2/2 + gz)(out)$

Therefore, the First Law equation becomes:

$\dot{q}(in) = -\dot{m}(air)\big(h(in) - h(out)\big)$, or

$\mathbf{\dot{q}(in) = -\dot{m}(air)\, cp\, (T(in) - T(out))}$

Here, all the above terms denote the same physical quantities as described previously but are valid for the air element control volume. T(in) and T(out) are the temperatures of the air flowing in and out of the air control volume respectively.

The above equation governs the heat transfer occurring between the air and the core with the air element as the control volume.

3.3 Heat in Transit from the Surface of the Core Element to the Air

During the exhaust cycle (as is considered for this analysis), the air flowing through the channels of the core absorbs heat from it by the mode of convection, which is shown in the following equation:

$$\dot{q}(\mathbf{conv}) = \mathbf{h}.\mathbf{As}.(\mathbf{Tc} - \mathbf{Ta})$$

Where

$\dot{q}(\mathrm{conv})$: Heat transfer rate between the core element surface and the air flowing past it.

h: Heat transfer coefficient between the core element surface and the air flowing past it.

As: Surface area of contact between core element and air element.

Tc: Temperature of core element.

Ta: Temperature of the air flowing adjacent to the core element.

The heat transfer rate obtained in all three cases is equal, since the energy dissipated from the core element is the same as the energy absorbed the air flowing in and out of the control volume that is adjacent to the core element, and it is the same energy which is depicted in the third case as energy in transit from the core to the air.

CHAPTER 4: EXPERIMENTATION AND ITS DATA ANALYSIS TO UNDERSTAND THE THERMAL BEHAVIOR OF THE FBR

This chapter is intended to provide in-depth analysis of the results obtained from the experiment performed on the FBR setup with the objective of developing a better understanding of its thermal behaviour. The thermal behaviour is understood in terms of the air temperature trends, core temperature trends and the effectiveness trends, all of which are interlinked and are an integral part of the operation of the FBR. The air flowing through the channels of the core continuously exchanges energy with it and changes its own temperature as well as that of the core as it passes through. The temperatures of both the air and of the core change with respect to time as well as with respect to distance. The sensible effectiveness is a performance metric of the device whose value depends on the absolute temperature difference of the flowing air at the inlet and at the discharge. The sensible effectiveness is indicative of how much energy can be exchanged between the air and the core as a proportion of the maximum energy transfer that is theoretically possible considering the indoor and outdoor temperature limits. Therefore, the trends observed in the air and core temperature distributions eventually reflect in the trends observed for sensible effectiveness.

Through core temperature measurements and studying their variation with respect to the time for which the experiment was conducted paved way for a more accurate determination of the onset of pseudo steady state, which was earlier determined by observing the degree of alignment of the air discharge temperature trends during successive supply and successive exhaust cycles. The facilitation of core temperature measurements also made possible the direct comparison between air discharge temperature vs time variation and core temperature vs time variation during supply/exhaust cycles that in turn gave clarity on how energy transfer is occurring between the core and the air flowing through it and on the phenomena of charging and discharging of the core.

4.1 Experimental Setup

Table 4.1: Summary of conditions prevalent during the experiment

Parameter	Value
Chamber space temperature (outdoors)	95 F
Laboratory space temperature (indoors)	70 F
Temperature difference between simulated outdoors and indoors- ΔTmax (°F)	25 F
Duration of experiment	30 minutes

Figure 4.1 shows the side view of the FBR core with orientations of the different thermocouples installed on the core, while Figure 4.2 shows the view of the FBR core from the chamber side with the 16 thermocouples attached. For instance, the terms "Core Temp 41" or "Core Temp 11" refer to the temperature values at the core centre on the lab side and at the core centre on the chamber side respectively.

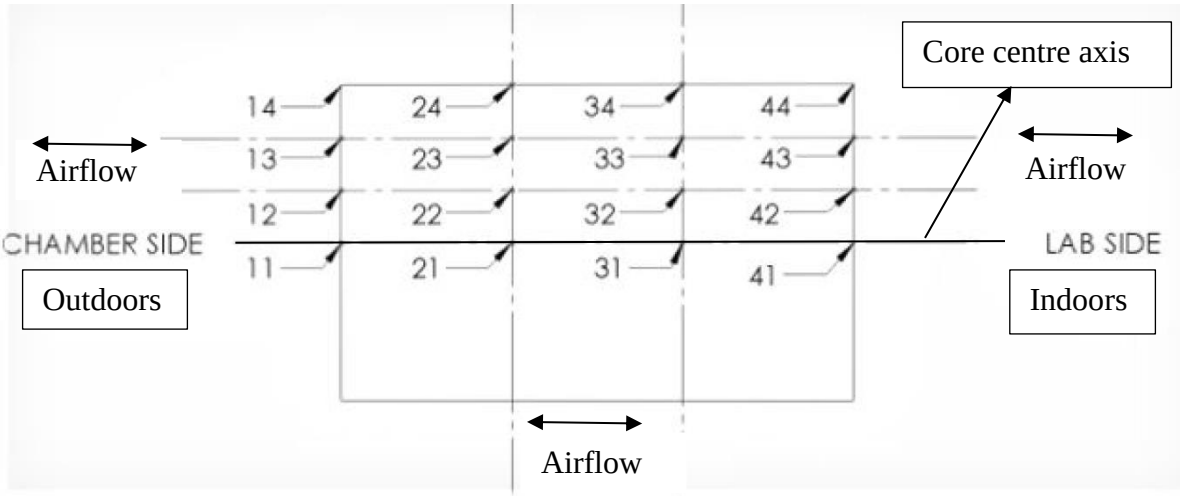

Figure 4.1: Schematic of the FBR core during the 16 point test with thermocouples attached at the locations shown.

Figure 4.2: FBR core from the chamber side with thermocouples attached at 16 points

Following is the nomenclature followed for the different core distribution sets analysed in the report, as will be evident in the plots shown.

11-21-31-41: Core Centre
12-22-32-42: Core Centre mid
13-23-33-43: Core Top mid
14-24-34-44: Core Top

11-12-13-14: Core chamber
21-22-23-24: Core chamber mid
31-32-33-34: Core lab mid
41-42-43-44: Core lab

For the air temperature measurements, there was one thermocouple positioned on the supply (lab) side of the FBR and one on its exhaust (chamber) side.

4.2 Results and Inferences

Shown in Figure 4.3 is the variation of the air temperature at the lab side and at the chamber side with respect to test time. A general observation is that the discharge temperature during supply cycle going into the lab space increases as the cycle progresses and the discharge temperature

during exhaust cycle going into the chamber space decreases as the cycle progresses. This means that the absolute temperature difference between the air at the inlet and at the discharge reduces with time during a particular cycle- this is because the "charging" and "discharging" rate of the core decreases with time- the energy exchange capacity of the core with the air flowing through it decreases with time, during the cycle.

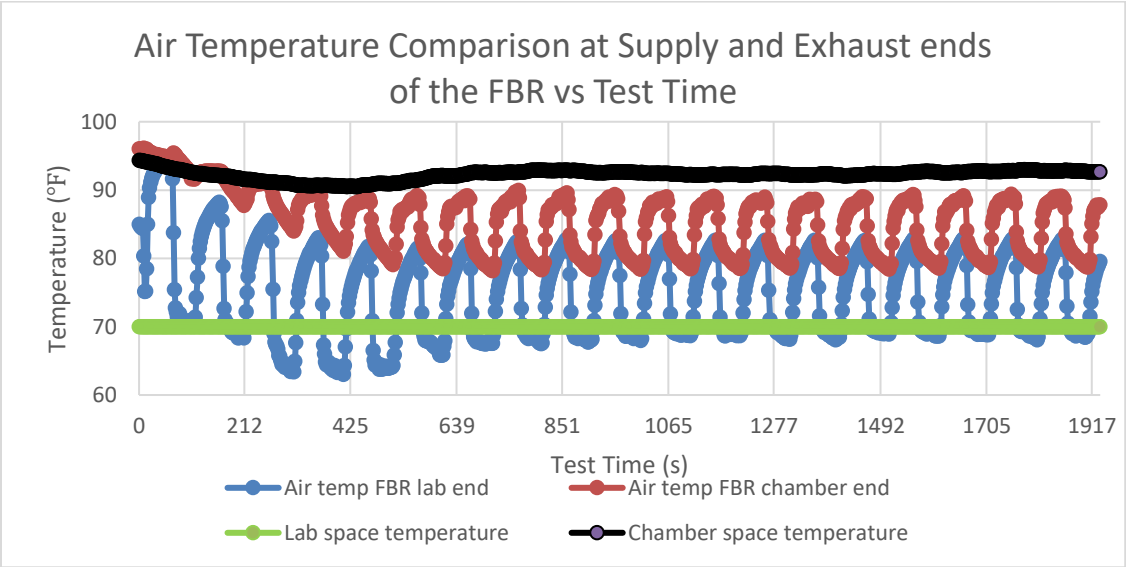

Figure 4.3: Air Temperature Comparison at Supply and Exhaust ends of the FBR vs Test Time

Figure 4.4 shows the core temperature variations with test time, at different locations of the unit. From visual inspection of the trendlines, one can get a good idea of when the pseudo steady state is attained. These curves have a downward incline after the experiment is started. However, these curves "flatten" out with time and become horizontal around when Test time = 1000 seconds. It can be stated that this is an approximate time estimate of when pseudo steady state is attained, wherein the charging of the core during the supply cycle (temperature rise in the curve) is exactly balanced by the discharging of the core during the exhaust cycle (temperature drop in the curve). As expected, because of the chamber space being maintained at a higher temperature than the lab space, the mean core temperatures on the chamber side are higher than those on the lab side. (for instance, the blue lines corresponding to "Core Temp 11" (refer to Figure 4.1 for the nomenclature used for different core temperature locations) are always above the purple lines corresponding to "Core Temp 41"). This indicates a heat flow within the core from the exhaust side (chamber space)

to the supply side (lab space). Also, the fluctuations of the temperatures at the centre of the core on both the sides ("Core Temp 11" and "Core Temp 41") are noticeably larger than those at the top ("Core Temp 14" and "Core Temp 44"), which implies that the centre of the core is much more responsive to the phenomenon of charging and discharging than the top.

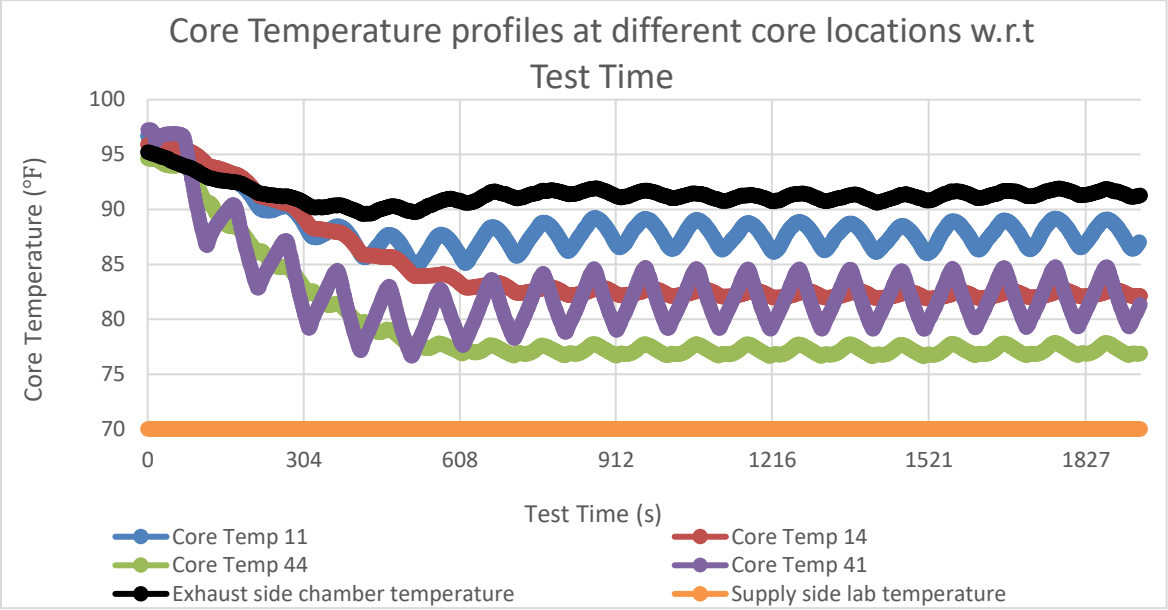

Figure 4.4: Core Temperature profiles at different core locations w.r.t Test Time

Figure 4.5 shows the variation of air discharge temperature for supply cycle followed by the same for the exhaust cycle during pseudo steady state. During the supply cycle, the core takes up heat from the air flowing through the unit, reducing the air temperature as it enters the lab space. As the cycle progresses, the rate of energy transfer from the air to the core reduces that causes the temperature at the supply discharge to increase with time. In other words, the temperature difference between the air at the inlet of the FBR on the chamber side and at the discharge of the FBR on the lab side (air is flowing from the chamber side to the lab side during supply cycle) reduces with time since the core slows down its ability to cool the air flowing through it as time passes.

During the exhaust cycle, the core dissipates heat to the air flowing through the unit, thus raising its temperature as it enters the chamber side. As the cycle progresses, the rate of heat transfer from

the core to the air reduces that causes the air temperature at the exhaust discharge to decrease with time. In other words, the temperature difference between the air at the inlet of the FBR on the lab side and at the discharge of the FBR on the chamber side (air is flowing from the lab side to the chamber side during exhaust cycle) reduces with time since the core slows down its ability to heat the air flowing through it as time passes.

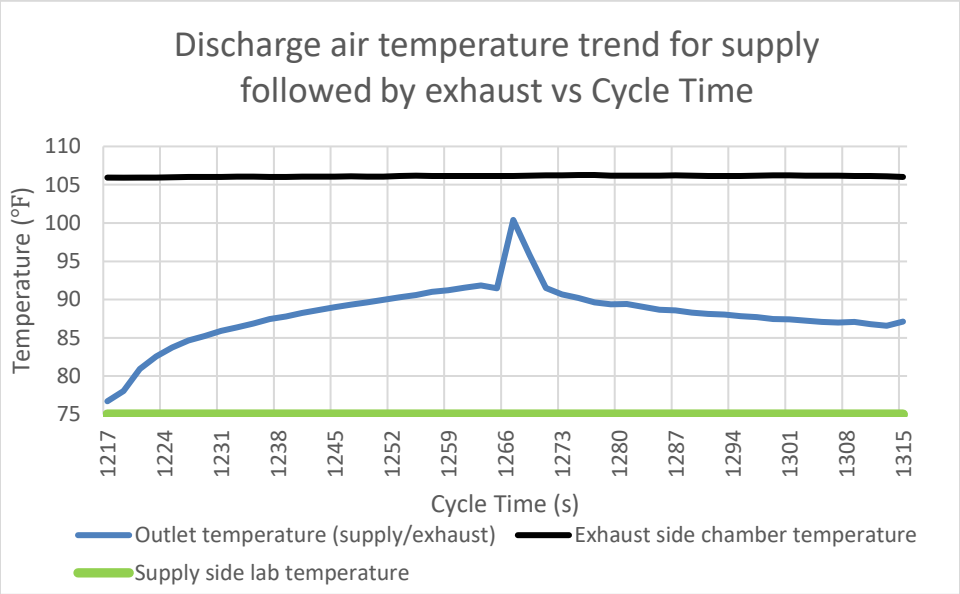

Figure 4.5: Variation of air discharge temperature for supply cycle followed by the same for exhaust cycle w.r.t Cycle time

Shown in Figure 4.6 is the variation of sensible effectiveness over a complete cycle, starting with a supply cycle and followed by exhaust cycle. The four trendlines depict the effectiveness variation at different times during the test. The yellow line corresponding to the 13th and 14th minute of the test is when the FBR is approaching the pseudo steady state, and the grey line corresponding to the 21st and 22nd minute of the test is when the FBR is well within the pseudo steady state timeline. The two lines align very closely, as anticipated.

It should be noted that at the beginning of the test (3rd and 4th minute), the effectiveness for the supply cycle is significantly lower than that of the exhaust cycle. However, during the pseudo steady state, the effectiveness for the supply cycle becomes comparable to that of the exhaust. The decreasing effectiveness trend is in line with the fact that the absolute temperature difference between the air at the discharge and at the inlet of the FBR reduces as the particular cycle

progresses- this is caused due to the core's decreasing ability to exchange energy with the air flowing through it as time passes during a cycle.

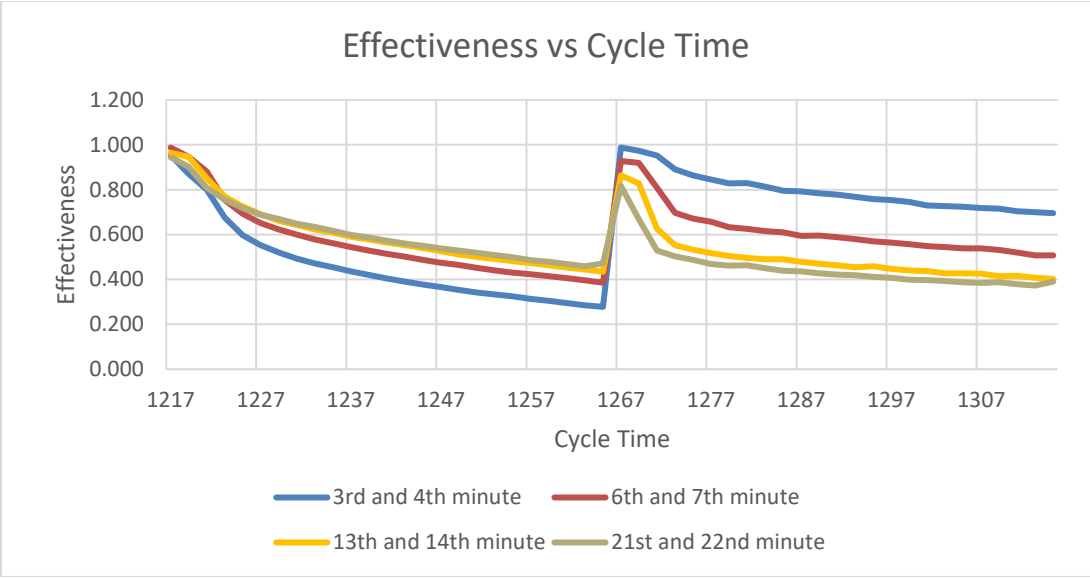

Figure 4.6: Effectiveness vs Cycle Time

Figure 4.7 shows the longitudinal core temperature variation for the supply cycle during the pseudo steady state (refer to Figure 4.1 and the nomenclature followed on page 30 for the different core distribution sets analysed). This variation is depicted for all longitudinal positions starting from the centre of the core to the top. "Core_centre_mid" and "Core_top_mid" denote the longitudinal positions just above the core centre and just below the core top respectively.

It can be seen that for all longitudinal positions (horizontal levels) starting from the core centre to the core top, the temperature shows a downward trend from the chamber side to the lab side. The downward trend can be explained by the fact that that air temperature at the chamber side end of the FBR is a lot higher than that at the lab side end of the FBR (downward air temperature distribution trend) , and for the core to take up heat from the moving air and cool it as it passes through its channels, the core longitudinal temperature distribution should also show a downward trend such that the core is taking up heat from the flowing air and "charging" throughout the length of the core. In other words, the longitudinal temperature trendline of the core should be below the one for the air for heat transfer to take place from the air to the core.

From a radial perspective, the temperatures at the core centre at the corresponding horizontal positions are the highest (red trendline), and gradually decrease as the radius increases and are the lowest at the top of the core (blue trendline).

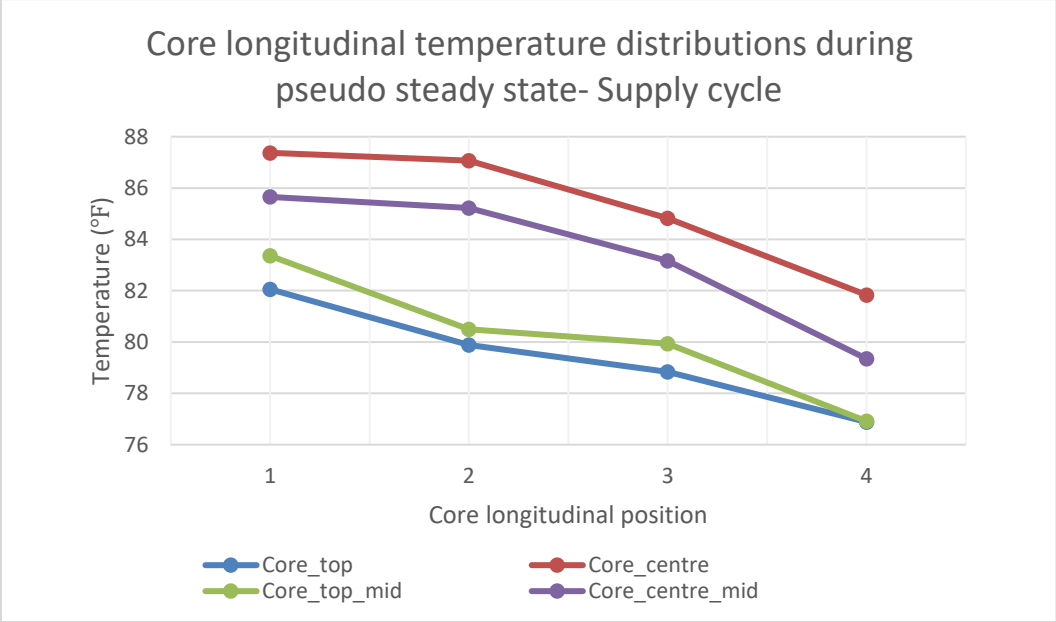

Figure 4.7: Core longitudinal temperature distributions during pseudo steady state- Supply cycle

Figure 4.8 shows the longitudinal core temperature variation for the exhaust cycle during the pseudo steady state (refer to Figure 4.1 and the nomenclature followed on page 30 for the different core distribution sets analysed).

It can be seen that for all longitudinal positions (horizontal levels) starting from the core centre to the core top, the temperature shows a downward trend from the chamber side to the lab side, or in other words, an upward trend from the lab side to the chamber side. This can be explained by the fact that air temperature at the lab side is significantly lower than that at the chamber side (upward air temperature distribution trend from lab side to chamber side) , and for the core to give up heat to the moving air and heat it as it passes through the channels of the core, the core longitudinal temperature distribution should also show an upward trend (from lab side to the chamber side) such that the core is “discharging” at all longitudinal positions. In other words, the longitudinal temperature trendline of the core should be above the one for the air for heat transfer to take place from the core to the air.

From a radial perspective, the temperatures at the core centre at the corresponding horizontal positions are the highest (blue trendline), and gradually decrease as the radius increases and are the lowest at the top of the core (purple trendline). One exception would be that the core temperature at the core chamber centre and at the point on the core chamber side corresponding to "Core centre mid" are coincident. (blue and red trendlines at the left end of the graph)

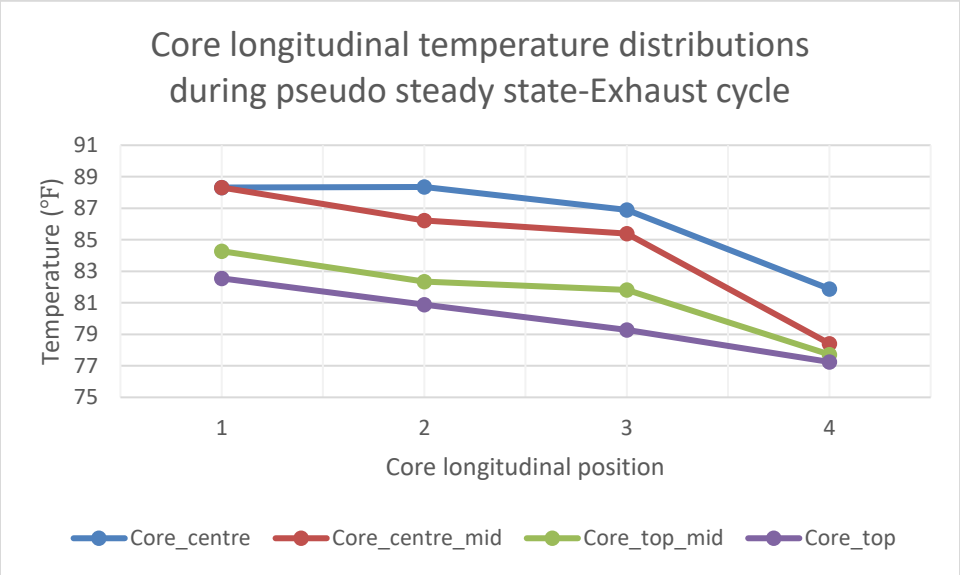

Figure 4.8: Core longitudinal temperature distributions during pseudo steady state-Exhaust cycle

Shown in figure 4.9 is the radial temperature distribution against the core radial position for the supply cycle during the pseudo steady state (refer to Figure 4.1 and the nomenclature followed on page 30 for the different core distribution sets analysed). Each of the trendlines corresponds to the four points at which core temperature is measured; for better visualization, these points can be imagined to lie on vertical lines perpendicular to the longitudinal axis of the core (please refer to FBR schematic and the nomenclature). These vertical lines are equidistant from each other across the core length.

It can be observed (for all the four vertical imaginary lines) that the temperature decreases from the centre of the core to its top. One possible explanation could be that the air flowing through the core has higher velocity at the centre and it gradually decreases as one goes further outwards towards the radius of the core, which implies that, because the heat transfer coefficient between the air and the core is proportional to the velocity of the flowing air, the heat transfer rate to the

core from the air is highest at the centre and it gradually decreases with radial distance, with it being at its minimum at the top of the core. A higher heat transfer rate from the air to the core is indicative of a higher core temperature attained.

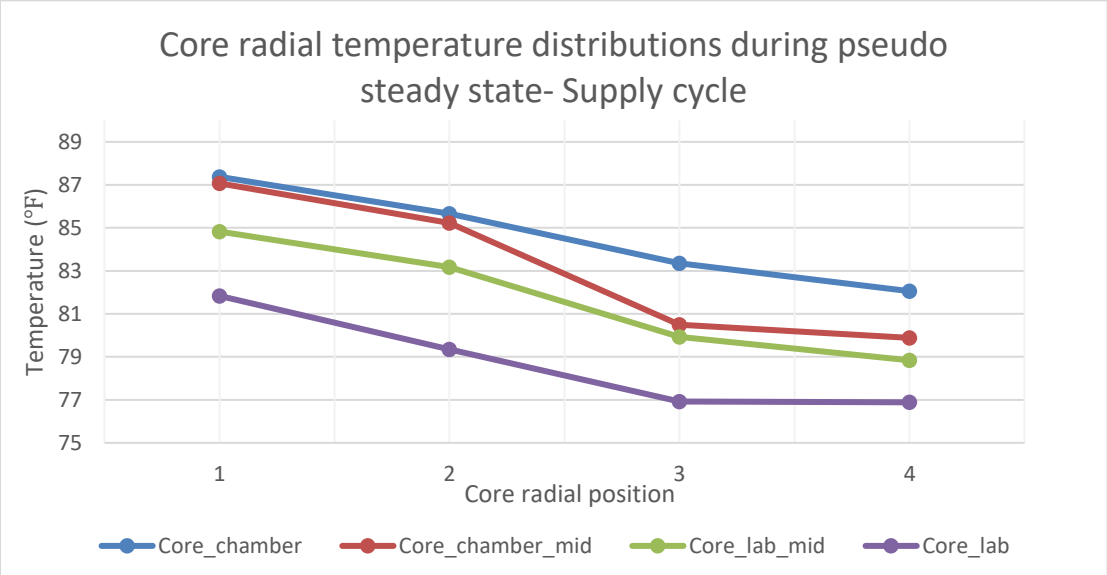

Figure 4.9: Core radial temperature distributions during pseudo steady state- Supply cycle

Figure 4.10 shows the radial temperature distribution against the core radial position for the exhaust cycle during the pseudo steady state (refer to Figure 4.1 and the nomenclature followed on page 30 for the different core distribution sets analysed). One can observe that the temperature decreases from the centre of the core to its top. One exception would be that the core temperature at the core centre on the chamber end and at the point on the core axis corresponding to “Core centre mid” are coincident. (blue and red trendlines at the left end of the graph)

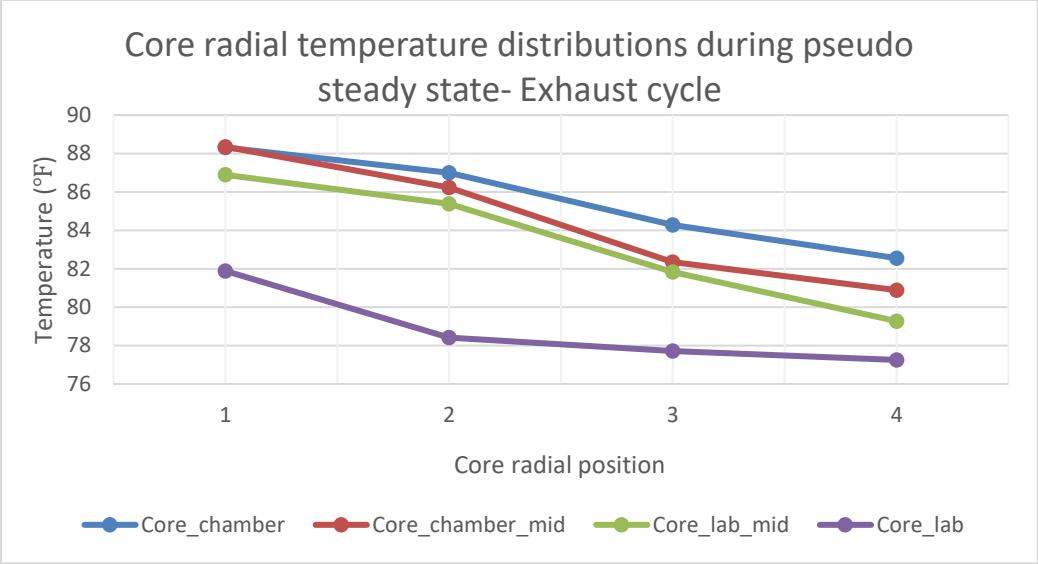

Figure 4.10: Core radial temperature distributions during pseudo steady state- Exhaust cycle

Shown in Figure 4.11 are the time varying temperature profiles (during supply cycle) at the four different equidistant locations of the core on the lab side (refer to Figure 4.1), and their comparison with the time varying temperature profile for air (red trendline) on the supply side (lab side), when the air is flowing from the chamber space to the lab space. All of the core temperature trendlines show an upward trend which justifies the charging phenomenon of the core during the supply cycle.

However, the core centre temperature on the lab side Core Temp 41 (refer to Figure 4.1 for the nomenclature used for different core temperature locations) , as indicated by the dark blue line, is always higher than the supply air discharge temperature on the lab side. Also initially, this air discharge temperature is lower than all the other four core temperatures and it is only after around 8 seconds that it goes higher than all except for the core centre lab side temperature (dark blue line). This indicates that the heat transfer from the air to the core (charging) during the supply cycle is not taking place during the first few seconds; the heat transfer at a particular location begins only after the temperature of the air goes higher than the core temperature at that point.

After the 8 second mark, although the core centre on the lab side is not taking up heat from the air, all the other three core points are doing so. This suggests that for the bulk core temperature to increase during supply, it may not be necessary for all points on the core to absorb heat for the charging phenomenon to occur.

An alternate explanation for this air temperature trend could be that the thermocouple for air temperature measurement was not placed (due to structural constraints of the FBR) at the same longitudinal location as the core temperature measurement thermocouples- this is because the position of the reversible fan makes it difficult for the air temperature measuring thermocouple to be inserted near the location of the core temperature measuring thermocouple. This inaccuracy of the air temperature measurement could be the reason for the air discharge temperature to be lower than the core centre temperature on the lab side.

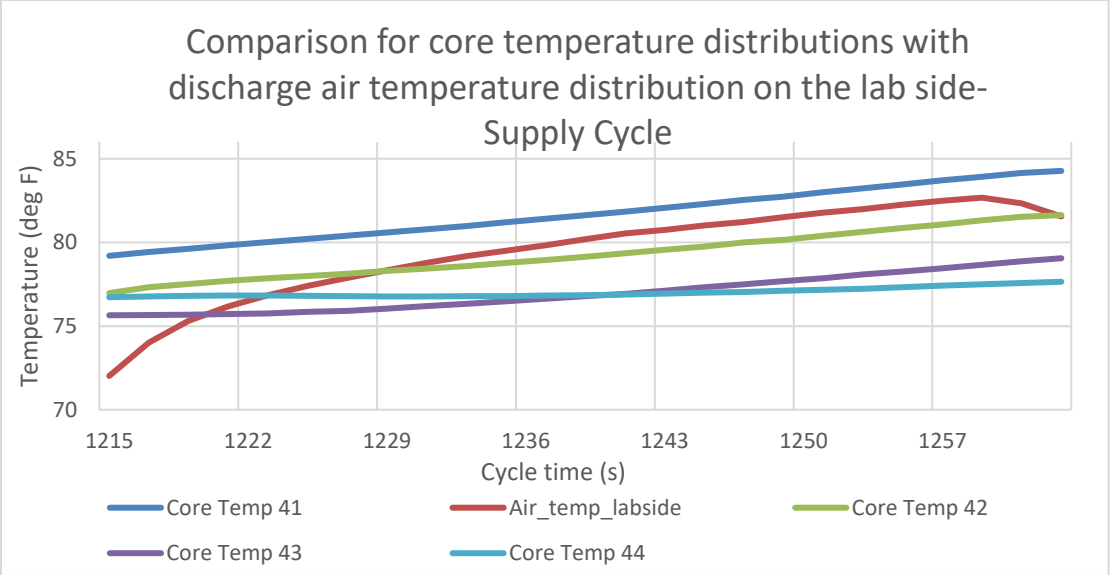

Figure 4.11: Comparison for core temperature distributions with discharge air temperature distribution on the lab side- Supply cycle

Figure 4.12 shows the comparison between the time variation of the air discharge temperature on the chamber side (light blue trendline) and the temperature at the centre of the core on the chamber side (red trendline), or Core Temp 11 (refer to Figure 4.1 for the nomenclature used for different core temperature locations) during the exhaust cycle. As anticipated, the core centre chamber side temperature shows a downward trend, indicating that the core is discharging and dissipating heat to the air. Moreover, this core centre temperature is always higher than the air discharge temperature, which reinforces the fact that the heat transfer is taking place from the core to the air, thus facilitating the discharging phenomenon.

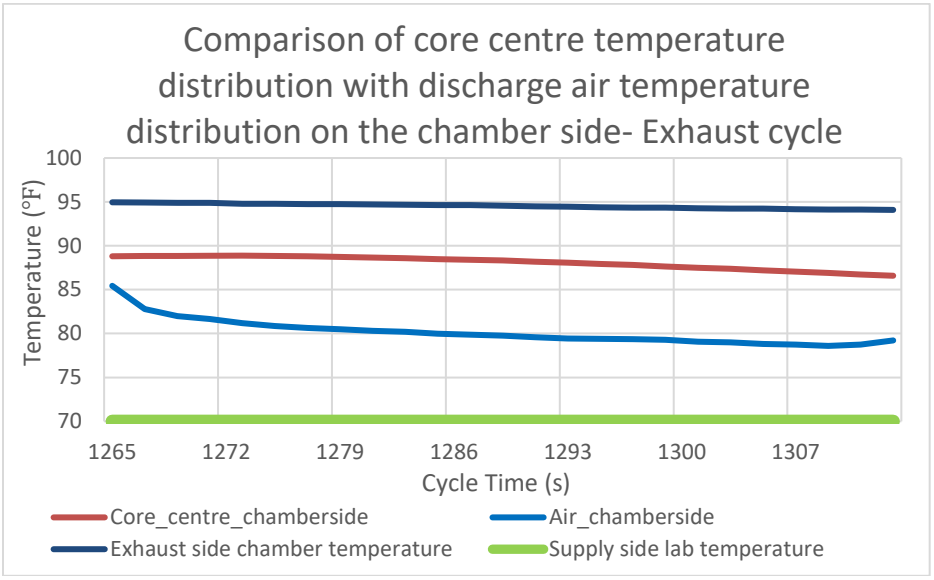

Figure 4.12: Comparison of core centre temperature distribution with discharge air temperature distribution on the chamber side- Exhaust cycle

Shown in Figure 4.13 is the time variation of core temperatures at different core locations against the cycle time for the supply cycle during pseudo steady state operation (refer to Figure 4.1 for the nomenclature used for different core temperature locations). The upward temperature trend that is prominently seen in the blue and purple lines, which correspond to core centre temperatures at the chamber side and lab side respectively, is indicative of the fact that the core is taking up heat from the air passing through its channels and is charging.

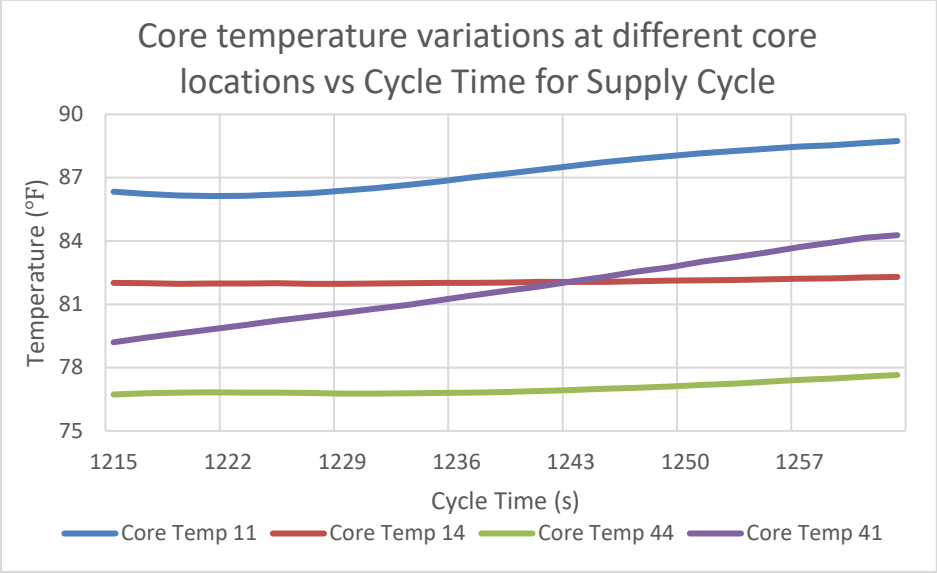

Figure 4.13: Core temperature variations at different core locations vs Cycle Time for Supply Cycle

Shown in Figure 4.14 is the plot of core temperature variations at different core locations against the cycle time for the exhaust cycle during pseudo steady state operation (refer to Figure 4.1 for the nomenclature used for different core temperature locations). The downward temperature trend that is prominently seen in the blue and purple lines which correspond to core centre temperatures at the chamber side and lab side respectively, is indicative of the fact that the core is dissipating heat to the air passing through its channels and is discharging.

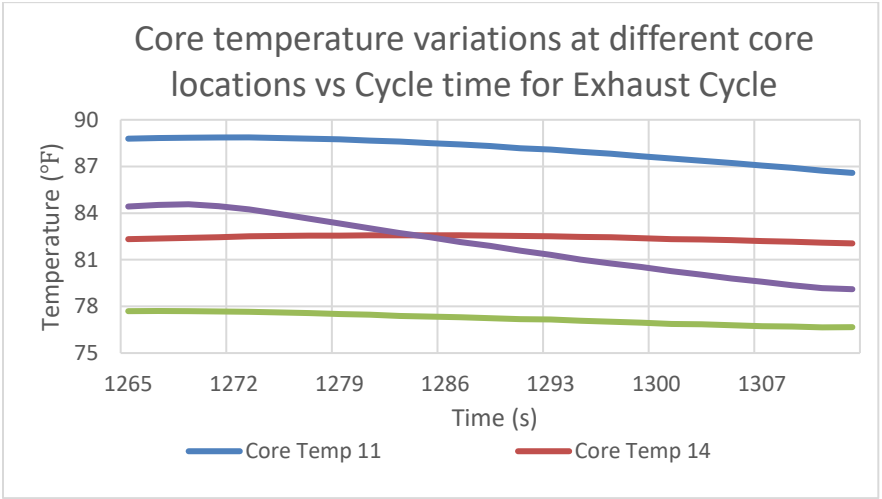

Figure 4.14: Core temperature variations at different core locations vs Cycle time for Exhaust Cycle

4.3 Summary

1. Pseudo steady state is estimated to be attained approximately 16 minutes after the experiment commences.

2. The mean core temperatures at various points on the chamber end of the FBR are higher than those at various points on the lab end of the FBR.

3. The core centre points at the chamber end and at the lab end of the FBR are more thermally responsive than the corresponding points at the top of the core (core centre points show larger temperature fluctuations than the latter).

4. The air discharge temperature during supply cycle decreases as time passes, and during exhaust cycle increases with time. This is indicative of the core's slowing ability of exchanging energy with the flowing air as time passes.

5. The sensible effectiveness decreases with time during both supply and exhaust. Its values during supply and exhaust are comparable.

6. The longitudinal core temperature distribution shows a downward trend as one goes from the chamber end of the FBR to the lab end- this is true for both supply and exhaust. The reason for this is that in order to facilitate the charging and discharging process of the core during supply and exhaust respectively, the core temperature has to align itself with the air temperature trend that decreases from the chamber end to the lab end of the FBR.

7. The radial core temperature distribution shows a downward trend from the centre of the core to its top, for both supply as well as exhaust.

8. The core temperatures at different core locations increase with time during the supply cycle (core charging). However, the air discharge temperature was found to be lower than the core temperature at the centre on the lab end of the unit, contrary to expectations from

theory. It was concluded that for charging to occur, the air temperature need not be higher than the core temperature at each and every point for the bulk core temperature to rise. An alternate explanation to justify the air discharge temperature trend observed could be the inaccuracy in its measurement due to structural constraints of the FBR.

9. The core temperatures at different core locations decrease with time during the exhaust cycle (core discharging), with the core centre temperature at the chamber end always higher than the air discharge temperature during exhaust.

CHAPTER 5: INFLUENCE OF INDOOR AND OUTDOOR TEMPERATURE LIMITS ON THE THERMAL BEHAVIOR OF THE FBR

The thermal behavior of the Fixed Bed Regenerator depends on several operating conditions, such as the air flow rate through the channels of the core from the indoors to the outdoors and vice versa, the temperature difference between the indoors and outdoors (which in the simulated experimentation scenario would be the lab space and the chamber space respectively), geometric parameters of the core (length, diameter), core material properties, and core thermodynamic properties (thermal conductivity).

This chapter aims to study the influence of the temperature difference between the indoors (lab space) and outdoors (chamber space) on the thermal behavior of the FBR. Broadly speaking, the thermal behavior of the FBR denotes the sensible effectiveness trends, air temperature profiles and core temperature profiles. This chapter looks at different ways of analyzing how ΔTmax (the temperature difference between indoors and outdoors) influences FBR behavior – comparison at different ΔTmax values is made between the air and core temperature swings on either ends of the FBR unit, mean core temperatures, air discharge temperatures during supply and exhaust, effectiveness variation with time, mean and peak effectiveness trends, core temperature variation with time, core temperature variation with longitudinal distance, etc. The mean and peak effectiveness trends are analyzed to determine the optimal operating conditions at which the FBR is at peak performance, where the performance metric used is effectiveness.

The effectiveness trends that are obtained from the experimental analysis are used as a basis to explain the air discharge temperature trends. The air inlet and discharge temperature trends are in turn used as a basis to explain the core temperature trends that are time and distance varying.

There were three experiments performed on the FBR experimental setup for this comparative study, where the ΔTmax in each experiment was varied. However, all the other operating conditions were kept constant in each experiment. Eventually, for the three experiments, the ΔTmax was maintained at 20°F, 25°F and 30°F. (shown in Table 5.1)

Table 5.1: ΔTmax values maintained during the three experiments, with their corresponding indoor and outdoor temperature limits.

ΔTmax (°F)	Indoor (Lab space) Temperature (°F)	Outdoor (Chamber space) Temperature (°F)
20	70	90
25	70	95
30	75	105

5.1 Results and Inferences

Figure 5.2 shows the variation of temperature swing for supply and exhaust air temperatures with respect to change in ΔTmax. Temperature swing is defined as the difference between the highest and the lowest air temperatures attained for either the lab end or the chamber end of the FBR unit (as shown in Figure 5.1- blue trendline refers to air temperature at the lab end of the unit, while the orange trendline refers to air temperature at the chamber end of the unit). It can be observed from Figure 5.2 that for the supply side air temperature (on the lab side), the swing shows a gradual linear increase from ΔTmax = 20°F to ΔTmax = 30°F. For the exhaust side air temperature (on the chamber side), though, the swing increases slightly from ΔTmax = 20°F to ΔTmax = 25°F but shows a sharp increase from ΔTmax = 25°F to ΔTmax = 30°F. As the ΔTmax increases (the upper and lower operating temperature limits of the FBR) the gap between the temperature limits experienced at either ends of the FBR (temperature swing) is also likely to increase.

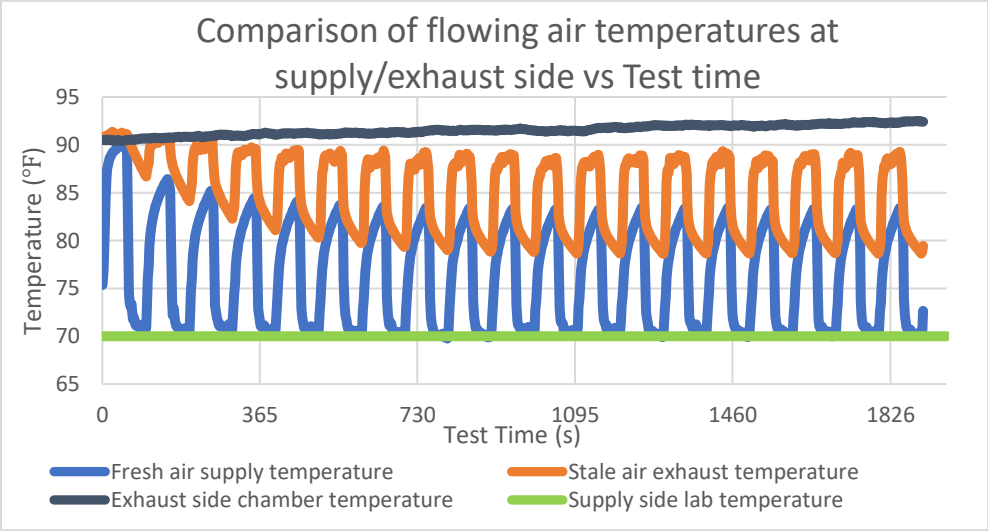

Figure 5.1: Variation of flowing air temperatures at the exhaust (chamber side) and at the supply (lab side) with Test time (for ΔTmax=20°F).

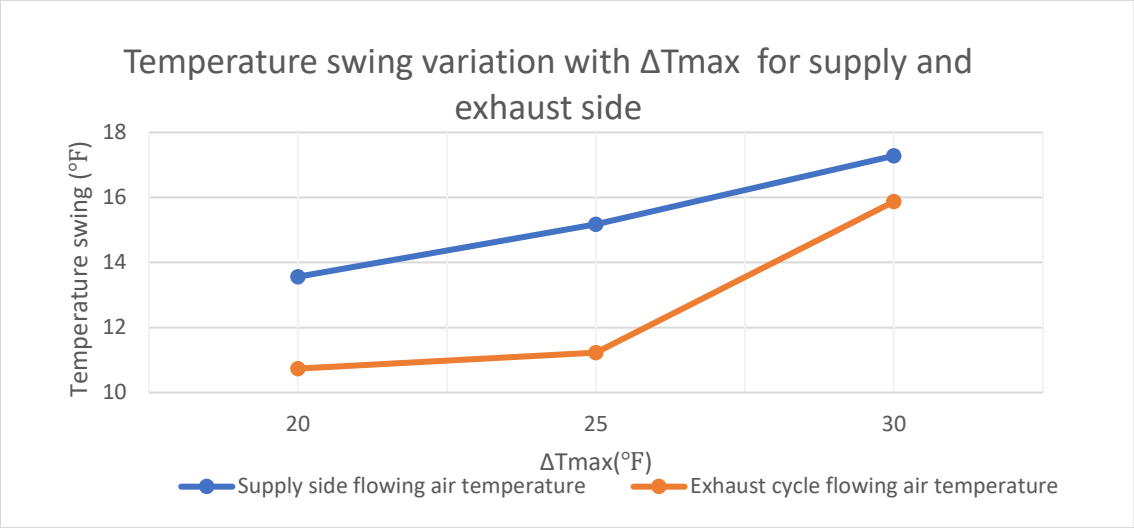

Figure 5.2: Variation of flowing air temperature swing with ΔTmax

Figure 5.5 depicts the core temperature swing variation with respect to ΔTmax, at both ends of the unit. Figures 5.3 and 5.4 illustrate the core temperature variations at the core chamber-side centre and at the core lab-side centre at the three ΔTmax values. The ceramic core of the FBR is in constant thermal interaction with the air flowing through its channels. As the temperature swing for the air temperatures at either ends of the FBR increases with ΔTmax (as shown in Figure 5.2), a given point on the core "adjusts" its temperature swing to align with the air temperature swings. Because of the "charging" and "discharging" phenomenon, the core has to maintain temperature swing trends which align with those of the air in order to ensure that its temperature at a particular location is above that of the flowing air during exhaust and below that of the flowing air during supply , although the difference between these two temperatures depends on the magnitude of heat transfer occurring between the air and the core (at that location) and ultimately the mean effectiveness at that particular ΔTmax.

It is evident from Figures 5.3 and 5.4 that the temperature swing fluctuations are more significant for Core Temp 41 (lab side core centre ; refer to Figure 4.1 for the nomenclature used for different core temperature locations) than for Core Temp 11 (chamber side core centre). This aligns well with the fact that the supply side air temperature (lab side) shows a higher swing than the exhaust side air temperature (chamber side) -this observation is valid for all three values of ΔTmax. This further shows how the core temperature trends are influenced by the air temperature trends.

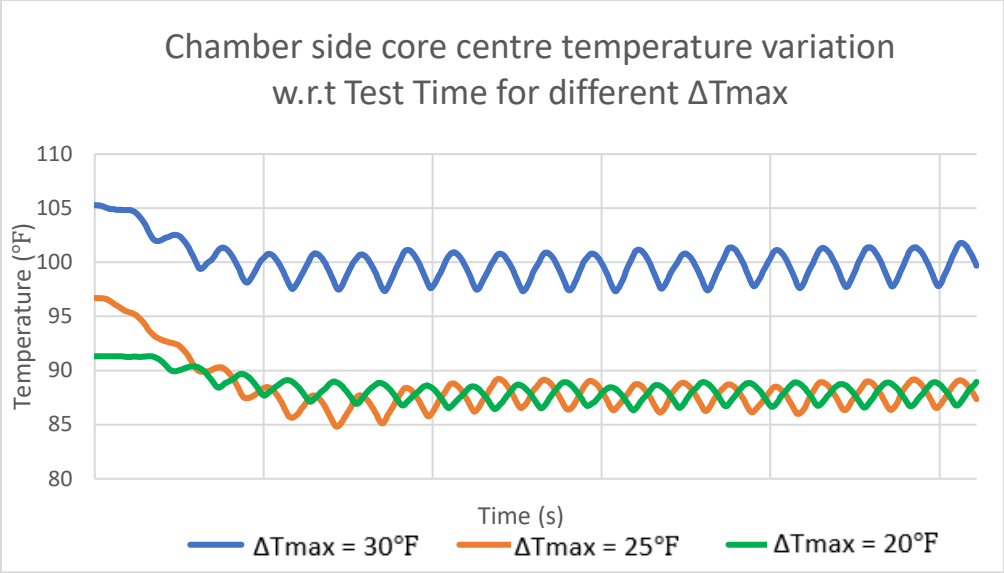

Figure 5.3: Chamber side core centre temperature variation w.r.t Test time at different values of ΔTmax.

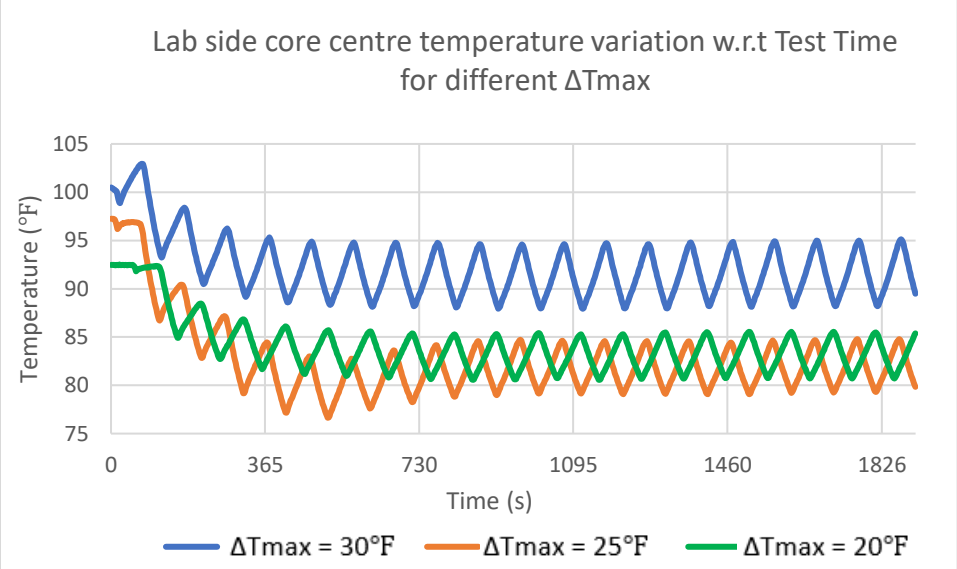

Figure 5.4: Lab side core centre temperature variation w.r.t Test time at different values of ΔTmax.

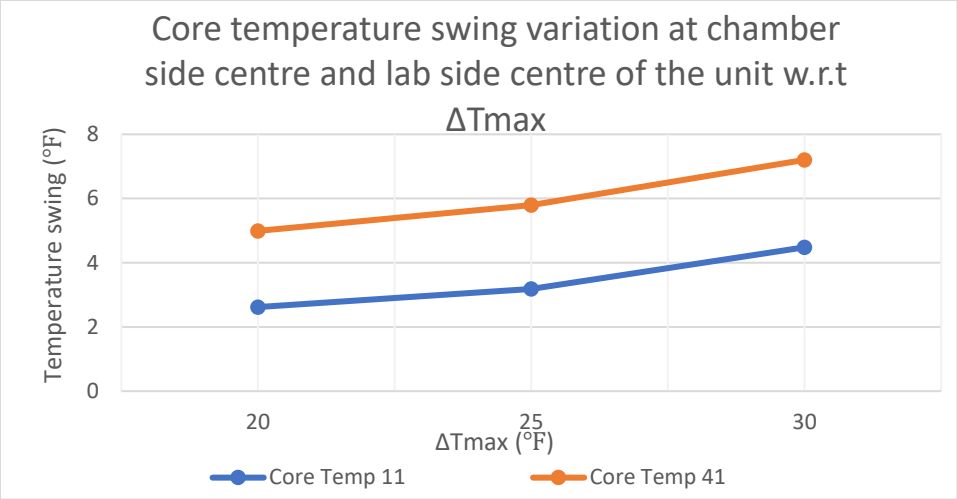

Figure 5.5: Core temperature swing variation at chamber side centre and lab side centre of the unit with ΔTmax.

As seen in Figure 5.6, mean core centre temperature on the chamber side Core Temp 11 (refer to Figure 4.1 for the nomenclature used for different core temperature locations) remains constant with an increase in ΔTmax from 20°F to 25°F, but sharply rises when ΔTmax=30°F. This sharp rise in the mean temperature can be due to the fact that the chamber space temperature at ΔTmax=30°F was kept at 105F, while it was kept at 90°F and 95°F during ΔTmax=20°F and 25°F respectively. This shows the effect that the chamber space temperature can have on the core temperature- a higher chamber temperature means that the air entering/exiting the core from the chamber side will be at a higher temperature, resulting in the core temperature being in a similar range. This effect, though, is not as prominently observed for a ΔTmax rise from 20°F to 25°F as much it is for a ΔTmax rise from 25°F to 30°F.

Mean core centre temperature on the lab side Core Temp 41 (refer to Figure 4.1 for the nomenclature used for different core temperature locations) decreases as ΔTmax increases from 20°F to 25°F, whereas it was expected that the temperature either remain constant because of the same lab side temperature maintained (70F) at ΔTmax=20°F and 25°F or it shows an increase as one goes from ΔTmax=20°F to ΔTmax=25°F, since the experiment performed at ΔTmax=25°F had a chamber space temperature of 95F as opposed to 90F maintained for the ΔTmax=20°F experiment. This decrease could be because the lab space temperatures recorded during the ΔTmax=20°F experiment dropped down below the 70°F limit; where 70°F was the pre-determined

lab space temperature limit during the experiment. The sharp rise observed in this mean core temperature with an increase in ΔTmax from 25°F to 30°F is as expected, because the lab space temperature at ΔTmax=30°F was maintained higher (75F) than for the experiments performed at ΔTmax=20°F and ΔTmaxmax=25°F experiments (70F for both).

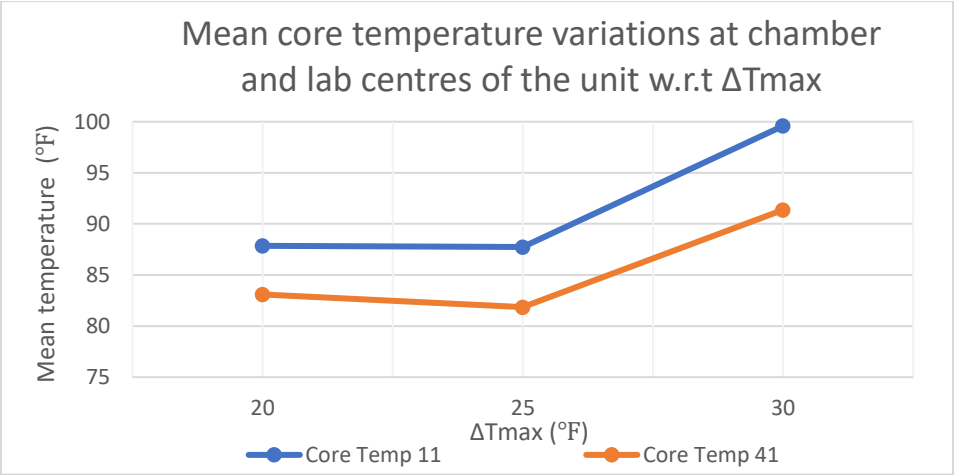

Figure 5.6: Mean core temperature variation at chamber side centre and lab side centre of the unit with ΔTmax.

Figure 5.7 shows the time – variation of the air discharge temperatures on the lab side during the supply cycle (left section of the plot) and on the chamber side during the exhaust cycle (right section of the plot).

The curve corresponding to ΔTmax=20°F is slightly above the curve corresponding to ΔTmax=25°F, with the ΔTmax=30°F curve being significantly higher than the other two. This difference is because of the higher chamber and lab side temperature limits maintained (75°F lab side, 105°F chamber side) during the ΔTmax=30°F experiment.

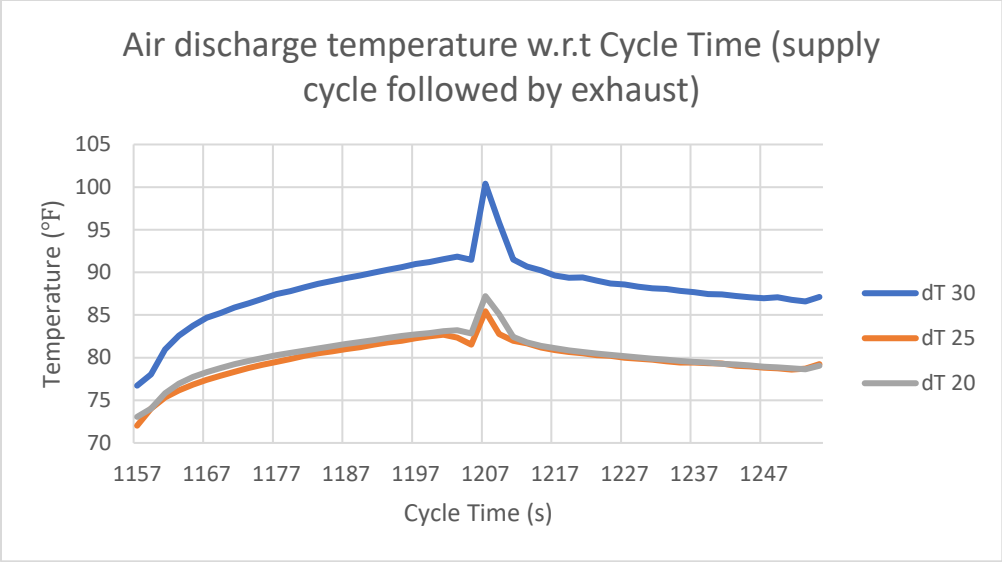

Figure 5.7: Air discharge temperature variation w.r.t complete Cycle Time (supply cycle followed by exhaust) for three different ΔTmax values.

It is observed from Figure 5.8 that the air discharge mean temperature for supply decreases when ΔTmax changes from 20°F to 25°F and sharply increases during the ΔTmax=30°F experiment. For exhaust, there is a marginal decrease as one goes from ΔTmax=20°F to 25°F, but again a sharp increase with a change in ΔTmax from 25°F to 30°F.

For exhaust, as seen in Figure 5.7, the temperature curve is marginally higher at ΔTmax=20°F than at ΔTmax=25°F. This makes sense because the mean effectiveness for exhaust is experimentally determined to be slightly higher at ΔTmax=20°F than at ΔTmax=25°F; the effectiveness for exhaust is proportional to the difference between the exhaust air outlet (chamber side) temperature and the lab space temperature (70°F).

For supply, as seen in Figure 5.7, the temperature curve is higher at ΔTmax=20°F than at ΔTmax=25°F. This again makes sense because the mean effectiveness for supply is experimentally determined to be lower at ΔTmax=20°F than at ΔTmax=25°F; the effectiveness for supply is proportional to the difference between the chamber space (outside) temperature (90F for ΔTmax=20°F and 95F for ΔTmax=25°F) and the supply air outlet (lab) temperature.

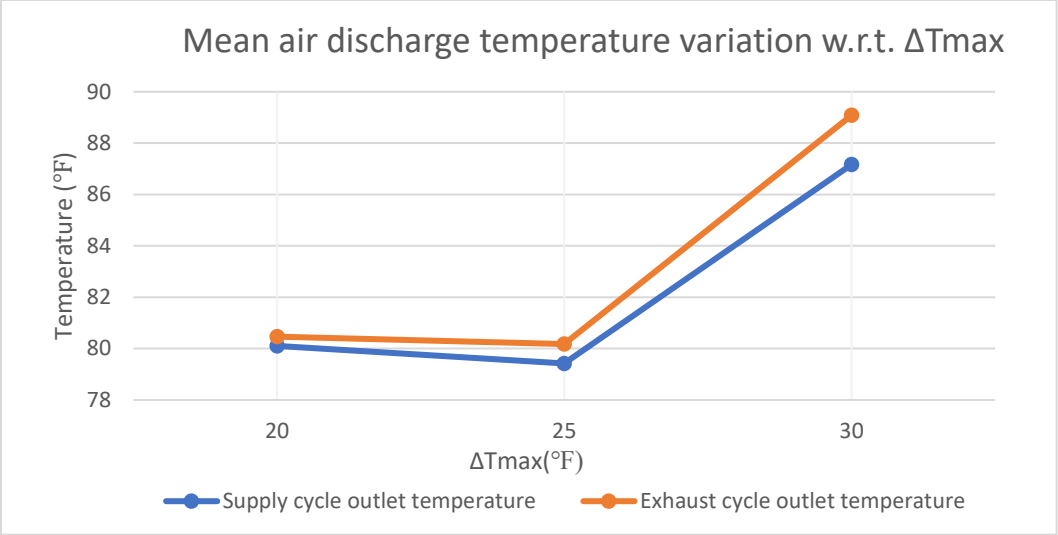

Figure 5.8: Mean air discharge temperature variation at different values of ΔTmax

Figure 5.9 shows the effectiveness trend during supply cycle at the three different ΔTmax values at which the experiments were performed. The effectiveness during the supply cycle at ΔTmax=30°F is the highest, followed by effectiveness at ΔTmax=25°F and then the one at ΔTmax=20°F. This order of effectiveness remains the same throughout the duration of the supply cycle.

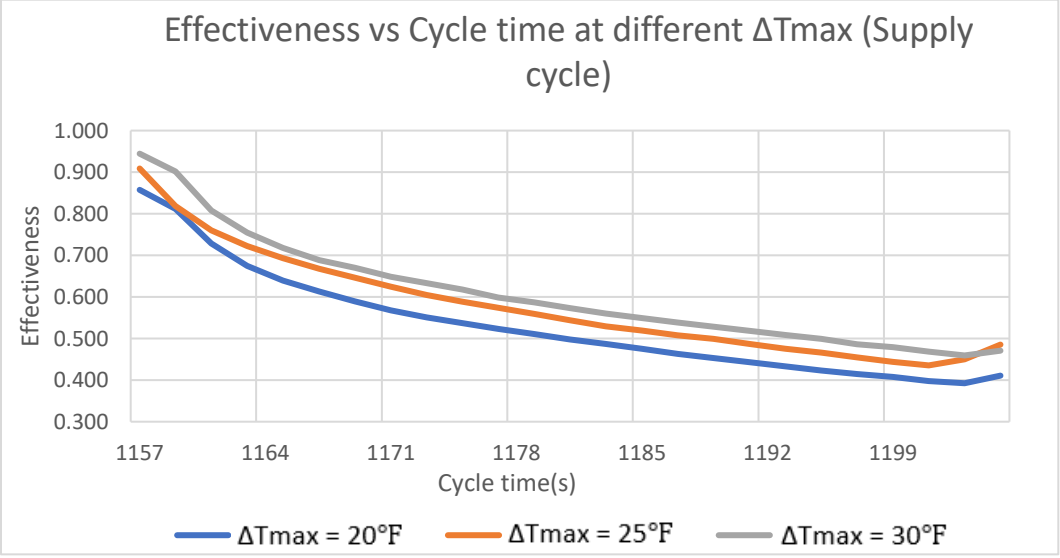

Figure 5.9: Effectiveness variation with cycle time for supply cycle at different ΔTmax

Shown in Figure 5.10 is the effectiveness trend during exhaust cycle at the three different ΔTmax values at which the experiments were performed. There is a sharp decline observed in the effectiveness at ΔTmax=30°F for the first few seconds of the cycle- starting from being the highest it drops down to being the lowest amongst the effectiveness trends corresponding to the three different ΔTmax values. For the remainder of the cycle, the order of effectiveness for the three ΔTmax values remains consistent- the effectiveness is highest for ΔTmax=20°F followed by effectiveness at ΔTmax=25°F, and the effectiveness for ΔTmax=30°F being the lowest.

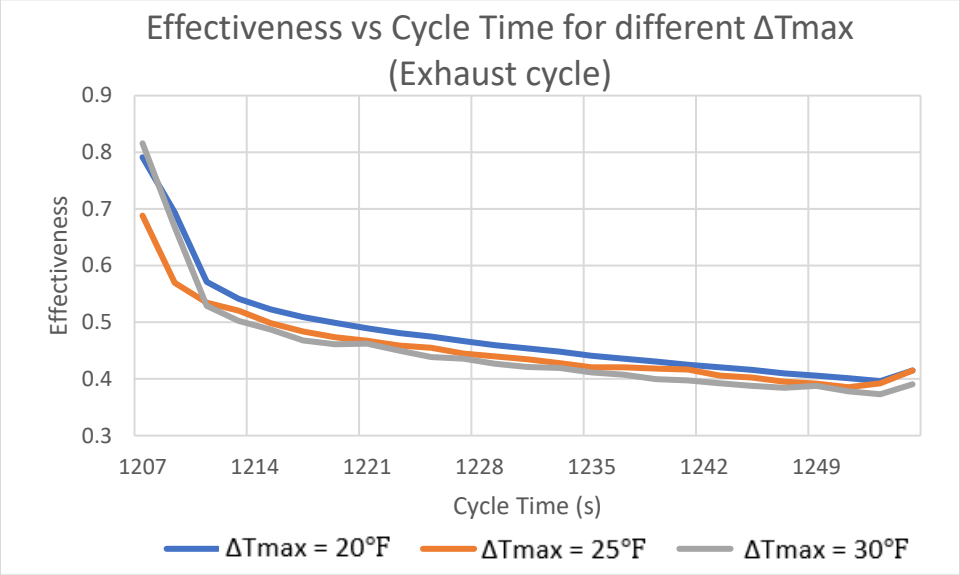

Figure 5.10: Effectiveness variation with cycle time for exhaust cycle at different ΔTmax

As seen in Figure 5.11, as ΔTmax increases from 20°F through 30°F the mean effectiveness shows a gradual rise during the supply cycle. However, for the exhaust cycle there is a decrease in mean effectiveness when there is a change in ΔTmax from 20°F to 25°F. A further rise in ΔTmax from 25°F to 30°F does not significantly impact the mean effectiveness, although there is a marginal decrease observed.

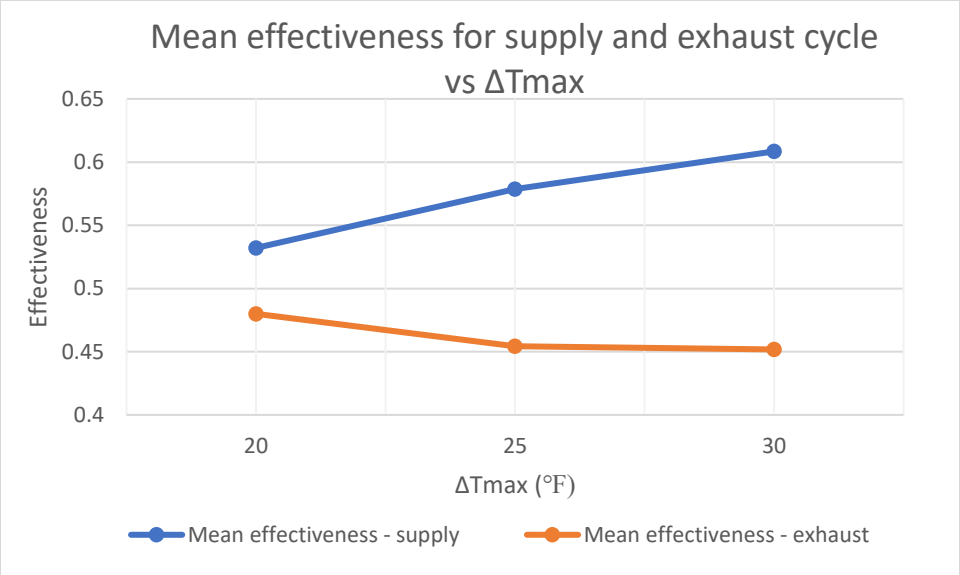

Figure 5.11: Mean effectiveness variation for supply and exhaust cycle w.r.t ΔTmax

Figure 5.12 shows peak effectiveness variation with ΔTmax for both the supply and the exhaust cycle. For the supply cycle, the effectiveness trend for both the mean and the peak values is the same – a gradual increase in effectiveness with increase in ΔTmax. However, for the exhaust, the peak effectiveness trend differs from the mean effectiveness trend. As mentioned before, at the start of the cycle, the effectiveness at ΔTmax=30°F is the highest, followed by effectiveness at ΔTmax=20°F and lastly the effectiveness at ΔTmax=25°F. It is important to compare values of peak effectiveness only at the start of a cycle, because the effectiveness during a particular cycle (supply or exhaust) always shows a downward trend with respect to cycle time.

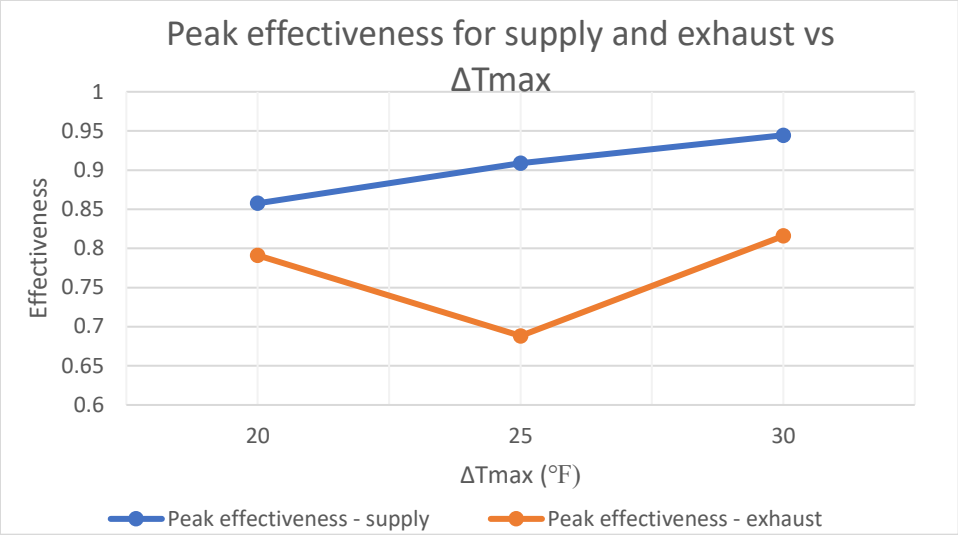

Figure 5.12: Peak effectiveness variation for supply and exhaust cycle w.r.t ΔTmax

Shown in Figure 5.13 is the comparison for mean effectiveness and peak effectiveness values during one complete cycle that comprises of a supply cycle followed by an exhaust cycle. As ΔTmax increases from 20°F upto 30°F, the mean effectiveness slows a slight but gradual increase, whereas the increase in peak effectiveness with increase in ΔTmax is more significant (the orange curve has a higher slope than the blue curve). Although it is important to study the performance of the FBR separately during supply and exhaust for more thorough analysis, observing the trend for one complete cycle gives a more comprehensive picture and helps in determining the optimum conditions of performance. At ΔTmax=30°F, the mean and the peak effectiveness values are at their respective maximum. It can be concluded that the best performance of the FBR is observed when ΔTmax=30°F, assuming all other parameters are unchanged between the experiments conducted at the three different ΔTmax values.

Although there is consistency in the mean and peak effectiveness trends observed for the supply cycle with those observed for the complete cycle (increasing trend in both the cases), the trends observed for the exhaust cycle are not consistent from those observed for the complete cycle.

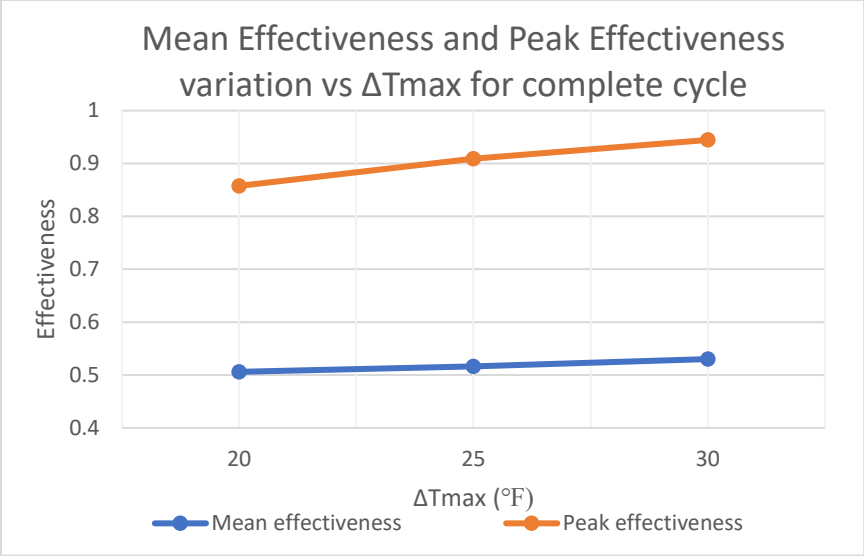

Figure 5.13: Mean and peak effectiveness variation for complete cycle w.r.t ΔTmax

Figure 5.14 shows the longitudinal core temperature distribution along the core centre axis, starting from the chamber end (left end of graph) to lab end (right end of graph) during supply cycle. At all the three ΔTmax values, the core temperature along the centre axis shows a downward trend from the chamber to the lab end. The blue and orange curves, corresponding to ΔTmax=20°F and ΔTmax=25°F respectively, are almost coincident for the core locations 11 and 21. At locations 31 and 41, the temperature corresponding to Tmax=25°F drops slightly below that corresponding to ΔTmax=20°F. The grey curve corresponding to ΔTmax=30°F is significantly above the other two- this is because of the relatively higher chamber space and lab space temperature limits of 105F and 75F respectively.

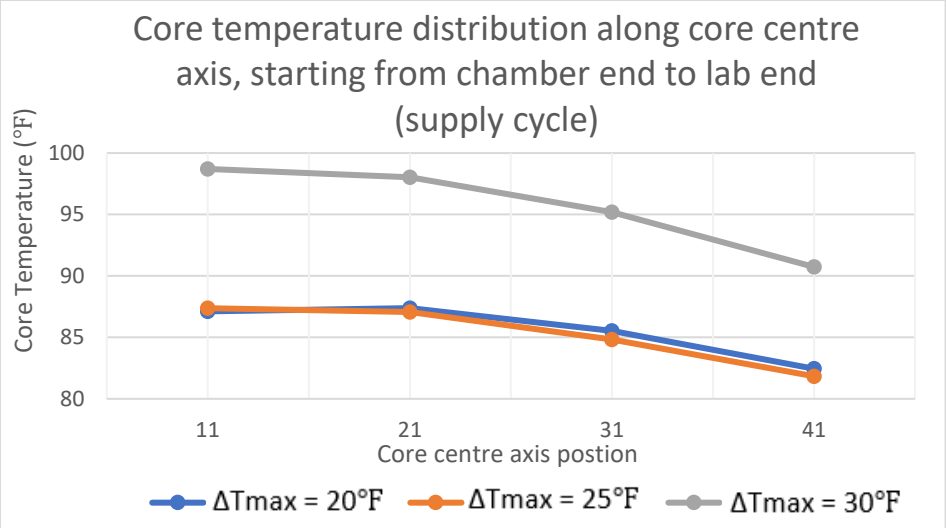

Figure 5.14: Core centre temperature distribution along equidistant points on the core longitudinal axis for supply cycle.

Shown in Figure 5.15 is the variation in the core centre temperatures at the chamber end and lab end w.r.t ΔTmax during supply cycle. Also shown in dotted lines are the temperatures of the flowing air at the chamber end and at the lab end (the air during supply flows from chamber end to the lab end).

The core centre temperature at the chamber end of the FBR (blue curve) remains constant with increase in ΔTmax from 20°F to 25°F and shows a sharp increase when ΔTmax=30°F. To explain this trend, the chamber side temperature of the air entering the unit (dotted grey curve) also shows a very similar trend as the one observed for the chamber side core centre, but the air temperature curve is slightly higher on the plot. Because of this, the energy transfer from the air to the core is made possible so that charging of the core occurs. The core temperature curve closely aligns itself with the air temperature curve because the two are in constant thermal interaction with one another for the charging to occur and the trend observed for the air temperature curve has to reflect in the one for the core temperature.

The core centre temperature at the lab end of the FBR (orange curve) experiences a very slight decrease with increase in ΔTmax from 20°F to 25°F and shows a sharp increase when ΔTmax=30°F. To explain this trend, the lab side temperature of the air exiting the unit also shows a very similar trend as the one observed for the lab side core centre. In contrast to expectations,

the air temperature curve (dotted yellow) is slightly lower than the core temperature curve on the plot. This implies that at this particular location (lab side core centre), energy transfer is actually occurring from the core to the air, whereas it was anticipated that the energy should have been transferred from the air to the core to facilitate charging of the core. This indicates that it is not necessary for every point on the core to take up energy from the air and to be "charged", as long as majority of the locations do take up energy from the core such that the bulk temperature of the core rises. Despite the above, the core temperature curve (orange curve) still closely aligns itself with the air temperature curve (yellow dotted) because the two are in constant thermal interaction with one another.

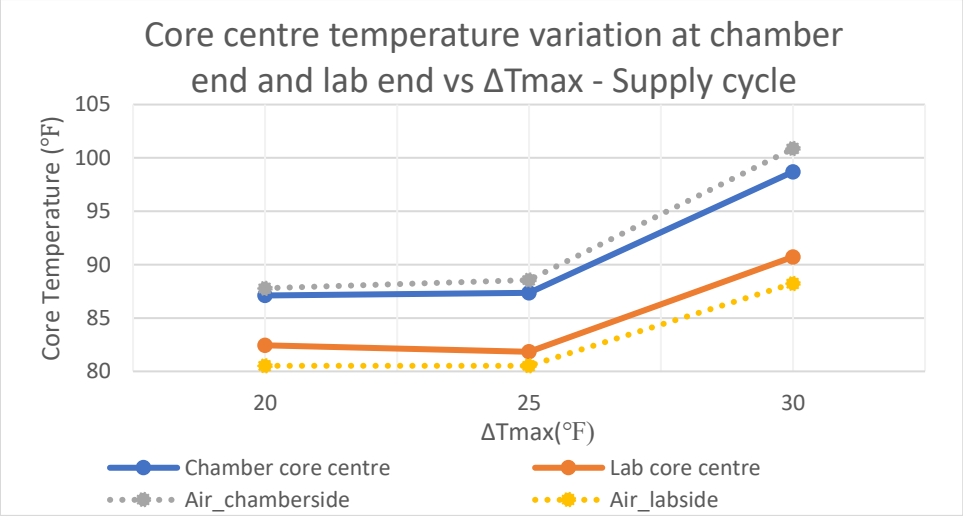

Figure 5.15: Core centre temperature variation w.r.t ΔTmax at chamber end and lab end during supply cycle

Figure 5.16 shows the longitudinal core temperature distribution along the core centre axis, starting from the chamber end (left end of graph) to lab end (right end of graph) during exhaust cycle. At all the three ΔTmax values, the core temperature along the centre axis shows a downward trend from the chamber to the lab end. The blue and orange curves, corresponding to ΔTmax=20°F and ΔTmax=25°F respectively, are almost coincident for the core locations 11 and 21. At locations 31 and 41, the temperature corresponding to ΔTmax=25°F drops slightly below that corresponding to ΔTmax=20°F. The grey curve corresponding to ΔTmax=30°F is significantly above the other two- this is because of the relatively higher chamber space and lab space temperature limits of 105F and 75F respectively.

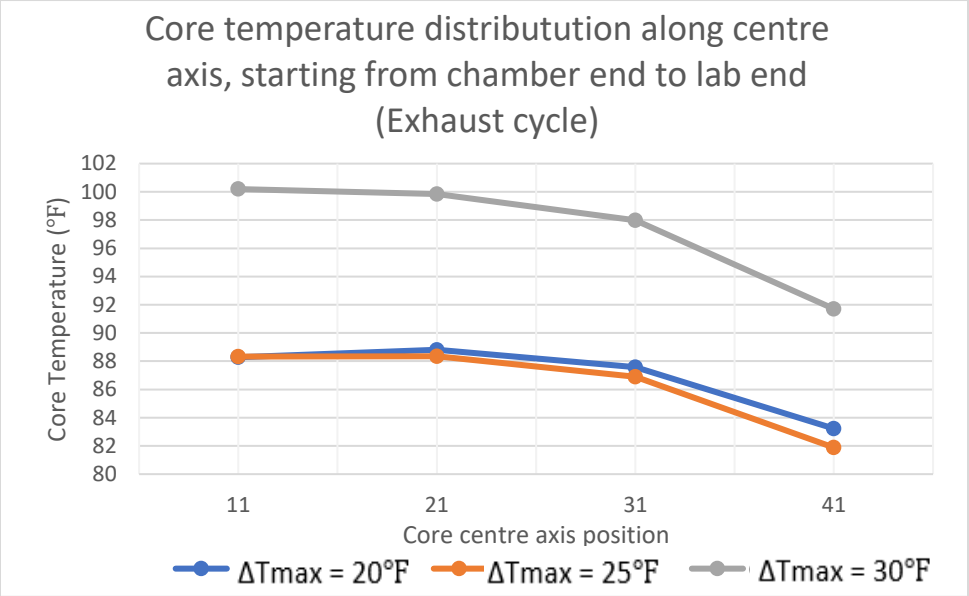

Figure 5.16: Core temperature distribution along equidistant points on the core longitudinal axis for exhaust cycle.

Shown in Figure 5.17 is the variation in the core centre temperatures at the chamber end (blue curve) and lab end (orange curve) of the unit w.r.t ΔTmax during exhaust cycle. Also shown in dotted lines are the temperatures of the flowing air at the lab end (air enters the FBR unit from the lab side) and at the chamber end (air exits the FBR unit and enters the chamber space).

The core centre temperature at the chamber end of the FBR (blue curve) remains constant with increase in ΔTmax from 20°F to 25°F and shows a sharp increase when ΔTmax=30°F. To explain this trend, the chamber side temperature of the air exiting the unit also shows a very similar trend to the one observed for the chamber side core centre temperature, but this air temperature curve (grey dotted curve) is significantly lower on the plot as compared to chamber core centre temperature curve (blue curve) . This facilitates energy transfer from the core to the flowing air, resulting in discharging of the core at its centre on the chamber side. The core temperature curve (blue) is aligned such that the core remains in constant thermal interaction with the air flowing through it channels.

The core centre temperature at the lab end of the FBR (orange curve) experiences a slight decrease with increase in ΔTmax from 20°F to 25°F and shows a sharp increase when ΔTmax=30°F. To

explain this trend, the lab side temperature of the air entering the unit also shows a very similar trend as the one observed for the lab side core centre temperature. As expected for exhaust cycle, the entering air temperature curve (dotted yellow) is noticeably lower than the core temperature curve on the plot. This implies that at this particular location (lab side core centre), energy transfer is occurring from the core to the air.

Thus, the reason for the core centre temperature on the lab side (orange curve) to trend the way it does is because of the particular trend observed for the entering air temperature from the lab side(yellow dotted curve), since the two are in constant thermal interaction with one another.

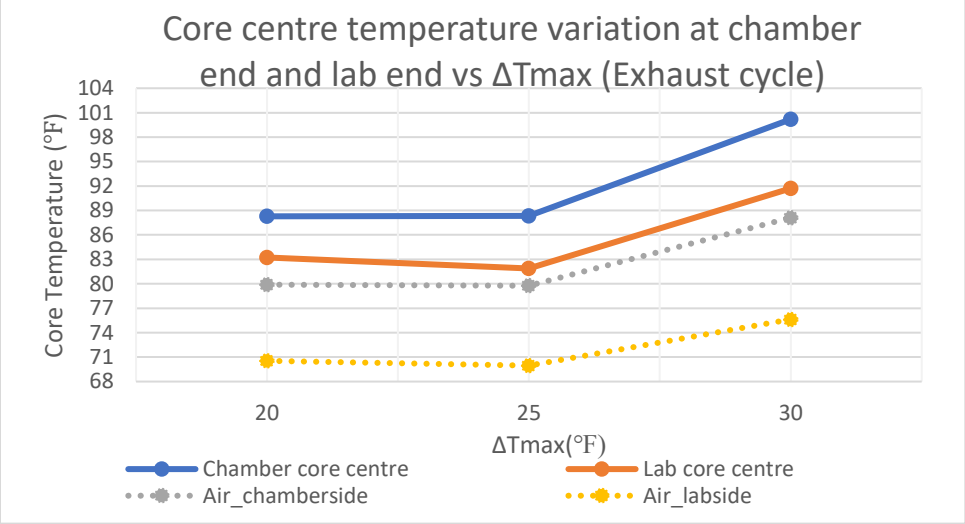

Figure 5.17: Core centre temperature variation w.r.t ΔTmax at chamber end and lab end during exhaust cycle.

Shown in Figure 5.18 is the time-variation of core centre temperature on chamber side during supply cycle for the three different ΔTmax values. Also shown is the time-variation of the temperature of air entering the unit from the chamber side (air flowing from chamber side to lab side) at the three ΔTmax values. It can be seen that for the most part of the cycle, the core temperature trendlines for all three ΔTmax values (blue, grey and orange trendlines) show a steady rise. This fits well with the fact that the core undergoes charging and its temperature increases. The lines corresponding to ΔTmax=20°F and ΔTmax=25°F almost coincide, but the one corresponding to ΔTmax=30°F is noticeably higher on the plot.

The air entering temperatures at the three ΔTmax values follow a very similar trend as compared to the corresponding core temperatures- this indicates that the core temperature trends are well aligned with the air temperature trends, as should be the case because the core is constantly exchanging energy with the air flowing through its channels. For ΔTmax=20°F and 25°F, the entering air temperature is lower than that of the core for the first few seconds, rises above it for around 20 seconds and then becomes equal to it. For ΔTmax=30°F, the entering air temperature is lower than that of the core for the first few seconds and then rises above it for the remainder of the cycle. From a theoretical perspective, though, the flowing air temperature should always be higher than the core temperature for the core to absorb energy from the air.

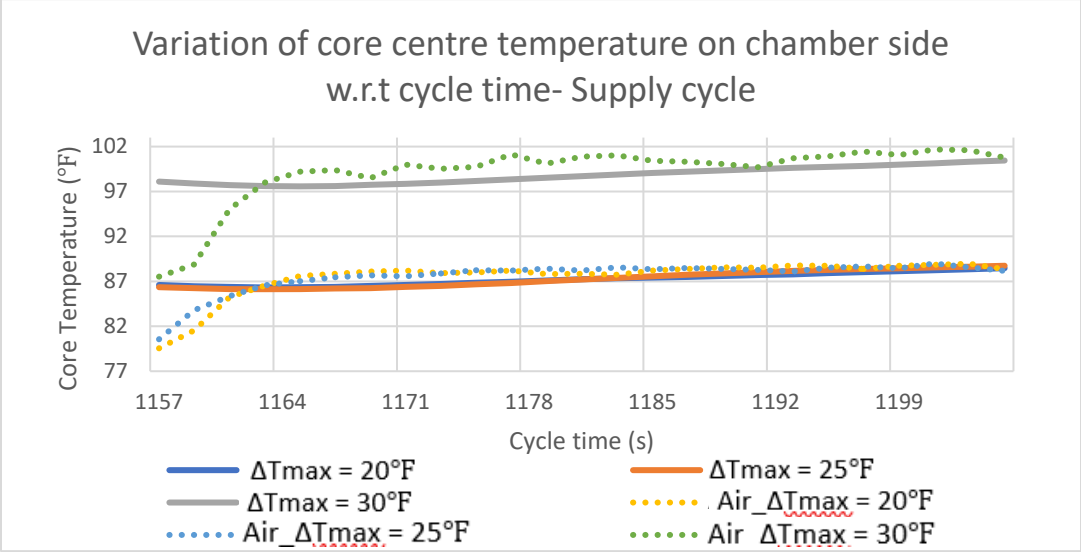

Figure 5.18: Core centre temperature variation on chamber side w.r.t Time during supply cycle at different ΔTmax.

Shown in Figure 5.19 is the time-variation of core centre temperature on lab side during supply cycle for the three different ΔTmax values. Also shown is the time-variation of the temperature of air exiting the unit from the lab side (air flowing from chamber side to lab side) at the three ΔTmax values. It can be seen that the core temperature trendlines for all three ΔTmax values (blue, grey and orange trendlines) show a steady rise throughout the duration of the cycle. This goes well with the fact that the core undergoes charging and its temperature increases. The line corresponding to

ΔTmax=20°F (blue curve) is slightly above the one corresponding to ΔTmax=25°F (orange curve), but the one corresponding to ΔTmax=30°F (grey curve) is noticeably higher on the plot.

The air exiting temperatures at the three ΔTmax values follow a very similar trend as compared to the corresponding core temperatures- this indicates that the core temperature trends are well aligned with the air temperature trends, as should be the case because the core is constantly exchanging energy with the air flowing through its channels. For ΔTmax=20°F and 25°F, the exiting air temperature is lower than that of the core throughout the cycle. It is also worth noting that the exiting air temperature trendline at ΔTmax=20°F is higher than the one at ΔTmax=25°F as was seen for the core temperature trendlines at ΔTmax=20°F and 25°F, thus reinforcing the fact that the core temperatures are well aligned with the air temperatures. For ΔTmax=30°F as well, the exiting air temperature is lower than that of the core throughout the cycle duration. As mentioned before, this is not in alignment with theoretical expectations, where the air temperature should be higher than the core temperature during supply cycle. At the same time, it is not a necessity for this order of air and core temperatures to be consistent at all points on the ceramic core, for its bulk temperature to increase.

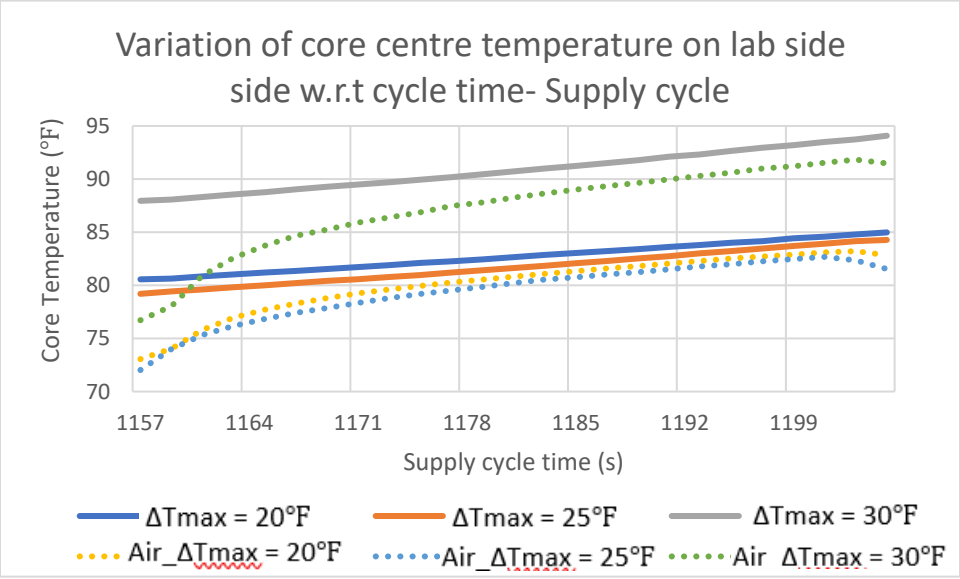

Figure 5.19: Core centre temperature variation on lab side w.r.t Time during supply cycle at different ΔTmax.

Figure 5.20 shows the time- variation of core centre temperature on chamber side during exhaust cycle for the three different ΔTmax values. Also shown is the time-variation of the temperature of air exiting the unit from the chamber side (air flowing from lab side to chamber side) at the three ΔTmax values. It can be seen that for the most part of the cycle, the core temperature trendlines for all three ΔTmax values (solid blue, grey and orange trendlines) show a steady decline. This aligns well with the fact that the core undergoes discharging and its temperature decreases. The curves corresponding to ΔTmax=20°F and ΔTmax=25°F almost coincide, but the one corresponding to ΔTmax=30°F is noticeably higher on the plot.

The air temperatures at the three ΔTmax values follow a very similar downward trend as compared to the corresponding core temperatures- this indicates that the core temperature trends are well aligned with the air temperature trends, because of which the discharging phenomenon (energy transfer from the core to the flowing air) is made possible. For ΔTmax=20°F and 25°F, the air temperature is lower than that of the core, and the corresponding trendlines are coincident (dotted blue and dotted yellow) , just like their core counterparts. For ΔTmax=30°F as well, the air temperature is lower than that of the core throughout the cycle. These observations align well with the theory, according to which during exhaust, the air temperature should always be lower than the core temperature for the air to absorb energy from the core so that its temperature increases.

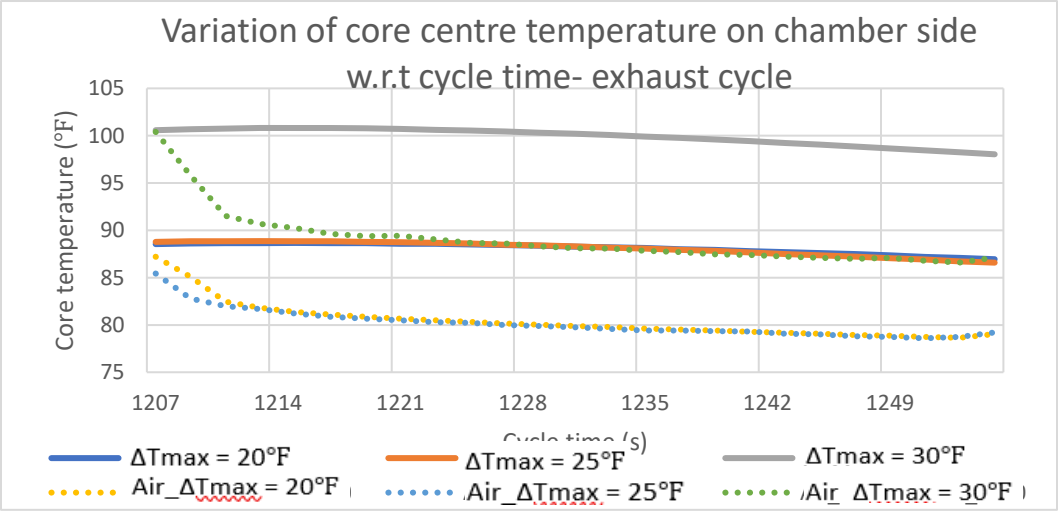

Figure 5.20: Core centre temperature variation on chamber side w.r.t Time during exhaust cycle at different ΔTmax.

Shown in Figure 5.21 is the time-variation of core centre temperature on lab side during exhaust cycle for the three different ΔTmax values. Also shown is the time-variation of the air temperature entering the unit from the lab side (air flowing from lab side to chamber side) at the three ΔTmax values. It can be seen that for the most part of the cycle, the core temperature trendlines for all three ΔTmax values (blue, grey and orange trendlines) show a steady decline. The line corresponding to ΔTmax=20°F (blue line) is slightly above the one corresponding to ΔTmax=25°F (orange line), but the one corresponding to ΔTmax=30°F (grey line) is noticeably higher on the plot.

The air entering temperatures at the three ΔTmax values all show a drastic decline in the first few seconds of the cycle after which their corresponding curves follow a reasonably similar trend as compared to the corresponding core temperature curves, although the latter show a sharper decline as compared to the air temperature curves. For ΔTmax=20°F and 25°F, the entering air temperature is lower than that of the core. Furthermore, the air entering temperature curve for ΔTmax=20 is slightly above the curve for ΔTmax=25°F. The same order follows for the core temperature curves at the corresponding ΔTmax values. This observation places emphasis on the close association between the core and the air flowing through its channels, and that the thermal behavior of the core can be considered to be heavily influenced by that of the flowing air. For ΔTmax=30°F as well, the entering air temperature is significantly lower than that of the core throughout the cycle, and it is this temperature gradient between the two that drives energy transfer from the core to the air, causing the core to discharge.

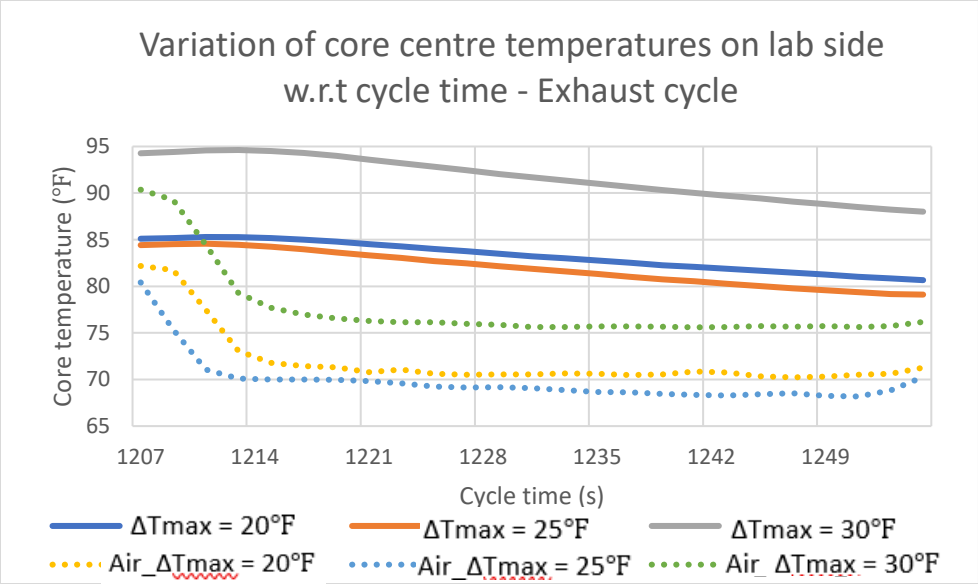

Figure 5.21: Core centre temperature variation on lab side w.r.t Time during exhaust cycle at different ΔTmax.

5.2 Summary

The FBR thermal behavior was analyzed with the objective of performing a comparative study at different indoor and outdoor temperature limits by focusing on the air temperature profiles, the core temperature profiles and the effectiveness trends. The air temperature profile comparative study (at the three ΔTmax values) comprised of observing the temperature swings on either side of the FBR unit, the discharge air temperature variation with time during supply and exhaust, and the mean discharge air temperatures during supply and exhaust. The core temperature profile comparative study focused on core temperature variation with longitudinal core position and time-varying temperature trends at different core locations. There were reasonings developed based on thermodynamics and heat transfer fundamentals to justify the trends observed. The time-varying effectiveness trends at the three ΔTmax values for supply and exhaust cycles were used as a basis to develop the variation of mean and peak effectiveness with ΔTmax . These trends were eventually used to determine the optimal operating conditions for the FBR at which peak performance is obtained.

CHAPTER 6: CONCLUSIONS

The Fixed Bed Regenerator (FBR) is a type of energy recovery system that offers preconditioning of fresh supply air without compromising on Indoor Air Quality (IAQ). The thermal behavior of a Fixed Bed Regenerator (FBR), operating as a heat recovery unit for buildings, was investigated by using a well-instrumented experimental facility that was specifically constructed to simulate real-world operations for energy efficiency. Experiments were conducted for a range of outdoor temperatures, which were simulated in a variable-temperature chamber, and a fixed indoor space temperature based on using lab-space air. These temperatures were controlled during experiments and then used to form three sets of indoor-to-outdoor temperature differences defined by ΔTmax values of 20°F, 25°F and 30°F. An analysis of FBR behavior in terms of measured temperatures for these three cases provided significant insights into the overall operation of the FBR.

As a first step, a methodology was developed for the determination of the onset of pseudo steady state, which was important because steady conditions were necessary before taking measured data to be used for analysis. In this light, steady conditions were achieved when core temperatures stabilized, and using this criteria, the onset of pseudo steady state was found to occur at around 16 minutes after the start of FBR operations for all three ΔTmax cases. The reason that it is necessary to use the word “pseudo” is that temperatures are always changing in an FBR as a result of cycling, with a complete cycle consisting of a combined supply and exhaust cycle, but at steady state the pattern of temperature changes become similar. Of special note, a complete cycle lasts about 100 seconds.

The core temperature trends on the chamber side (i.e, outdoors) were compared with the ones on the lab side (i.e, indoors). It was observed that during the pseudo steady state, the temperature fluctuations on the core center on the lab side (simulated indoor space) were higher than those on the core center on the chamber side (simulated outdoor space). When the core temperature values were observed at the middle of the cycle, the longitudinal core temperature distribution trends showed a downward trend from the chamber end of the unit to the lab end during both the supply and the exhaust cycles. This trend can be explained by the core temperatures having to closely align with flowing air temperatures at a given core location for the charging and discharging

phenomenon to occur. In other words, the core temperature has to be below the flowing air temperature at any given location during the supply cycle so that charging occurs. In contrast, during the exhaust cycle, the core temperature has to be above the flowing air temperature at any given location for discharging to occur. The net effect of the above processes is that the core temperatures monitored at different locations during the supply cycle increased with time (i.e, charging) whereas core temperature decreased with time (i.e, discharging) during the exhaust cycle, which aligns with theoretical concepts. Of importance and as mentioned earlier, the above results were obtained after pseudo steady state was reached.

An important goal of this study is to use the experimental data measured for the three ΔTmax cases to evaluate the FBR effectiveness, with the temperature change of air as it flows through the core channels being an indicator of effectiveness. For example, at the outdoor-to-indoor temperature difference case of ΔTmax =25°F, the air temperature difference between the inlet and the outlet during the supply cycle showed a 22.9°F to 11.8°F decrease from the cycle beginning to the cycle end. For the exhaust cycle, this difference decreased from 15.4°F at the cycle start to 8.6°F at the cycle end. This decreasing temperature difference from the start to the end of a cycle for both supply and exhaust cycles is indicative of the core's decreasing ability to exchange energy with the air or, of more importance in this study, a decreasing effectiveness as time passes during a cycle. The mean and peak effectiveness trends and values as ΔTmax is varied from 20°F to 30°F were also studied. Mean effectiveness for the supply cycle increased from 0.53 to 0.60 as the ΔTmax was varied from 20°F to 30°F. In contrast, the mean effectiveness for the exhaust cycle decreased from 0.47 at ΔTmax=20°F to 0.45 at ΔTmax=30°F. Peak effectiveness for the supply cycle increased from 0.85 to 0.94 as ΔTmax was varied from 20°F to 30°F, while for the exhaust cycle peak effectiveness increased from 0.79 to 0.81 as ΔTmax increased from 20°F to 30°F. When analyzing effectiveness for the complete cycle, both the mean and peak effectiveness increased with ΔTmax, and, in fact, reached maximums at ΔTmax=30°F with the maximum mean effectiveness for the complete cycle being 0.53 and the maximum peak effectiveness being 0.94. Also of note, mean effectiveness for the supply cycle was observed to be greater than for the exhaust cycle at all ΔTmax values.

REFERENCES

1. Ramin, H., Krishnan, E. N., & Simonson, C. J. (2020, June 30). *Effectiveness of fixed-bed regenerators for energy recovery in buildings applications*. E3S Web of Conferences. Retrieved March 5, 2023, from https://www.e3s-conferences.org/articles/e3sconf/abs/2020/32/e3sconf_nsb2020_09001/e3sconf_nsb2020_09001.html

2. Ramin, H. (2021, December 1). *Transient analysis and optimization of fixed-bed regenerators for HVAC applications*. HARVEST. Retrieved March 5, 2023, from https://harvest.usask.ca/handle/10388/13717

3. Chen, J., Liu, Y., & Lai, H. (2018). A review of thermal energy storage in buildings: Part 1. Unfired systems. Renewable and Sustainable Energy Reviews, 81, 1702-1725.

4. Zhu, Y., Zhang, C., Wang, X., & Huang, X. (2020). A comprehensive review of fixed-bed thermal energy storage for solar heating and cooling applications. Applied Energy, 262, 114509.

5. Li, Y., Li, X., Li, Y., & Wang, R. Z. (2016). Fixed bed regenerator for solid sorption refrigeration: a review. Renewable and Sustainable Energy Reviews, 60, 1282-1295.

6. Wu, D., Wu, G., Liu, X., Zhang, Q., & Yu, Y. (2019). Numerical and experimental study on a novel fixed bed regenerator incorporated with phase change material for enhancing thermal energy storage. Applied Thermal Engineering, 150, 70-81.

7. Zhang, J., He, Y. L., & Wang, R. Z. (2016). Performance investigation of a compact adsorption chiller with a fixed-bed regenerator using zeolite-water pair. Applied Thermal Engineering, 100, 1087-1096.

8. Gao, Y., Li, Z., Li, X., Huang, L., Wang, R. Z., & Li, Y. (2020). Improving the performance of fixed bed regenerators for thermal energy storage by adding graphene oxide. Applied Energy, 278, 115666.

9. Karami, H., Mohamadi, M., Kaviri, A. G., & Moghadam, A. N. (2019). Experimental investigation of a fixed-bed regenerator for preheating fresh air in commercial buildings. Energy and Buildings, 195, 61-69. doi: 10.1016/j.enbuild.2019.04.039

10. Zhao, Y., Li, X., Wu, Z., Wu, J., & Lu, Y. (2016). Experimental investigation on a fixed-bed regenerator for heat recovery in residential ventilation systems. Applied Thermal Engineering, 93, 986-994. doi: 10.1016/j.applthermaleng.2015.10.056